Research Square

Preprints are preliminary reports that have not undergone peer review.
They should not be considered conclusive, used to inform clinical practice,
or referenced by the media as validated information.

CD2AP Positively Regulates TGF-β1/Smad3-Mediated EMT via TβRI: A Novel Oncogenic Axis Driving Hepatocellular Carcinoma Progression

Dexi Wang
Affiliated Hospital of Traditional Chinese Medicine of Xinjiang Medical University
Xinran Meng
Tianjin University of Traditional Chinese Medicine
Fangfang Fan
Affiliated Hospital of Traditional Chinese Medicine of Xinjiang Medical University
Dina Tuerhong
Affiliated Hospital of Traditional Chinese Medicine, Xinjiang Medical University
Yuxuan Li
Affiliated Hospital of Traditional Chinese Medicine, Xinjiang Medical University
Jing Liu
Affiliated Hospital of Traditional Chinese Medicine of Xinjiang Medical University
Shengjun Zhao
Affiliated Hospital of Traditional Chinese Medicine of Xinjiang Medical University
Haiying Zhang
1030737878@qq.com

Affiliated Hospital of Traditional Chinese Medicine, Xinjiang Medical University

Research Article

Keywords: Hepatocellular carcinoma, CD2AP, TGF-β1/Smad3 signaling pathway, Epithelial-mesenchymal transition, TβRI, Therapeutic target

Posted Date: May 22nd, 2026

DOI: https://doi.org/10.21203/rs.3.rs-9398634/v1

License: This work is licensed under a Creative Commons Attribution 4.0 International License.
Read Full License

Additional Declarations: No competing interests reported.

CD2AP Positively Regulates TGF-β1/Smad3-Mediated EMT via TβRI: A Novel Oncogenic Axis Driving Hepatocellular Carcinoma Progression

Dexi Wang[a,b,1], Xinran Meng[c,1], Fangfang Fan[a], Dina Tuerhong[d], Yuxuan Li[a], Jing Liu[a], Shengjun Zhao[a,b*], Haiying Zhang[d*]

[a] *Department of Pharmacy, Affiliated Hospital of Traditional Chinese Medicine of Xinjiang Medical University, Urumqi, China;*

[b] *Xinjiang Key Laboratory of Processing and Research of Traditional Chinese Medicine, Urumqi, China;*

[c] *Institute of Traditional Chinese Medicine, Tianjin University of Traditional Chinese Medicine, Tianjin, China;*

[d] *Office of Drug Clinical Trial Institution, Affiliated Hospital of Traditional Chinese Medicine, Xinjiang Medical University, Urumqi, China*

[1] These authors contributed equally to this work

* Corresponding author. **Haiying Zhang and Shengjun Zhao**

E-*mail address*: *1030737878@qq.com (H.Zhang) , 1519531677@qq.com (S. Zhao)*

ABSTRACT

Hepatocellular carcinoma (HCC) remains a leading cause of cancer-related death worldwide, underscoring the urgent need to identify novel drivers of its progression. We investigated the oncogenic role and molecular mechanism of CD2AP in HCC. Analysis of clinical cohorts showed that CD2AP is markedly overexpressed in HCC tissues and that its upregulation correlates with advanced tumour stage and worse overall, disease-specific and progression-free survival; CD2AP therefore functions as an independent prognostic factor for HCC patients. Functional enrichment of genes correlated with CD2AP revealed prominent involvement in EMT and TGF-β signalling. Genetic manipulation in HCC cell lines demonstrated that CD2AP was required for tumour cell proliferation, migration, invasion and EMT. Mechanistically, Co-IP confirmed a direct physical interaction between CD2AP and TβRI; integrated molecular docking and molecular dynamics simulations further validated a stable, high-affinity complex. CD2AP functions as a positive regulator of downstream TGF-β1/Smad3 signalling and the EMT programme in a TβRI-dependent manner, as shown by coordinated changes in TβRI protein abundance, Smad3 phosphorylation and EMT marker expression following manipulation of CD2AP levels. Consistent with the *in vitro* results, CD2AP silencing markedly suppressed HCC xenograft growth in nude mice, whereas its overexpression accelerated tumourigenesis; these effects were accompanied by corresponding alterations in tumoral TβRI/p-Smad3 levels and EMT markers. Together, our findings establish CD2AP as a critical upstream positive regulator of the TβRI/Smad3 axis and reveal a novel oncogenic cascade that promotes HCC aggressiveness through TGF-β1/Smad3-mediated EMT. Targeting the CD2AP–TβRI interaction therefore represents a promising therapeutic strategy for HCC.

Keywords: Hepatocellular carcinoma;CD2AP;TGF-β1/Smad3 signaling pathway;Epithelial-

mesenchymal transition;TβRI; Therapeutic target.

Introduction

Hepatocellular carcinoma (HCC), which constitutes approximately 90% of primary liver cancer cases, represents the third leading cause of cancer-related mortality globally. The persistently rising incidence and mortality rates of HCC underscore a significant and growing public health burden [1-3]. While clinical interventions—including surgical resection, local ablation, liver transplantation, and targeted therapies such as sorafenib—have improved outcomes for a subset of patients [4-6], the overall prognosis remains poor. This is largely attributable to the frequently asymptomatic nature of early-stage disease, leading to late diagnosis at intermediate or advanced stages for the majority of patients. Moreover, advanced HCC is often characterized by a high propensity for metastasis and the development of therapy resistance, culminating in a dismal 5-year survival rate below 30% [7-9]. Consequently, elucidating the complex molecular pathogenesis of HCC and identifying novel, effective therapeutic targets are of paramount clinical importance.

CD2-associated protein (CD2AP) is a multifunctional scaffold and adaptor protein that orchestrates diverse cellular processes—including signal transduction, cytoskeletal dynamics, cell adhesion, and membrane trafficking—by interacting with numerous signaling molecules via its SH3 domains and proline-rich motifs [10-18]. Intriguingly, the role of CD2AP in cancer is highly context-dependent, exhibiting both tumor-suppressive and oncogenic functions across different malignancies. For instance, CD2AP acts as a tumor suppressor in clear cell renal cell carcinoma and gastric cancer, where its low expression correlates with advanced disease, poor prognosis, and enhanced metastatic potential [19, 21-22]. Conversely, CD2AP appears to exert

oncogenic effects in lung adenocarcinoma and hepatocellular carcinoma, where its upregulation is associated with reduced survival, aggressive tumor behavior, and modulation of the tumor immune microenvironment [23, 24]. In colorectal cancer, CD2AP forms a complex with TKS4 to regulate cell migration and epithelial-mesenchymal transition (EMT) [20]. This tissue-specific functional duality underscores CD2AP's role as a pivotal, context-dependent regulator of tumor progression and therapy response.

The high metastatic potential of HCC is a major determinant of patient mortality. This aggressive phenotype is largely driven by the epithelial-mesenchymal transition (EMT), a fundamental process wherein epithelial cells lose polarity and cell-cell adhesion, acquire mesenchymal characteristics, and gain enhanced migratory and invasive capacities [25-27]. Critically, EMT is initiated in primary tumor cells prior to intravasation, serving as a core mechanism enabling metastasis [28-30]. Consequently, targeting EMT represents a strategic priority for curbing tumor invasion and dissemination. Transforming growth factor-β1 (TGF-β1) is a master regulator of EMT, primarily through the canonical TGF-β/Smad signaling pathway [31-33]. A previous study demonstrated that the C-terminal region of CD2AP binds directly to the cytoplasmic domain of TGF-β receptor type I (TβRI) in a kinase-dependent manner. In vivo evidence from TGF-β1 transgenic mouse models revealed that loss of CD2AP exacerbates podocyte injury and proteinuria, confirming its functional role in modulating TGF-β pathway activity in a physiological context [34]. Nonetheless, the precise molecular mechanism by which CD2AP regulates the TGF-β1/Smad axis to influence HCC progression remains entirely unexplored.

In this study, we first employed public transcriptomic datasets (including TCGA) to establish the clinical relevance of CD2AP overexpression in HCC and its association with poor

patient prognosis, preliminarily linking it to TGF-β1-induced EMT. Through functional experiments in HepG2 and LI-7 cell lines, we demonstrated that genetic manipulation of CD2AP expression profoundly affects HCC cell proliferation, migration, invasion, and EMT. We further identified a direct physical interaction between CD2AP and TβRI, and delineated that CD2AP positively regulates the activity of the TGF-β1/Smad3 signaling pathway and EMT phenotype via TβRI in HCC.These in vitro findings were corroborated in a nude mouse xenograft model, where CD2AP was shown to drive tumor growth in vivo via activation of the TGF-β1/Smad3-EMT axis. Our work comprehensively defines CD2AP as a novel and critical promoter of HCC progression, presenting it as a promising prognostic biomarker and a rationale for developing therapeutic strategies aimed at disrupting the CD2AP-TβRI interface.

2. Methods

2.1. Highlights

- CD2AP is frequently upregulated in HCC and acts as a robust diagnostic and independent adverse prognostic biomarker.
- CD2AP drives malignant phenotypes of HCC cells by promoting proliferation, invasion, migration, and EMT process.
- CD2AP directly binds to TβRI to form a stable high-affinity complex in HCC cells for the first time.
- CD2AP positively activates the TGF-β1/Smad3 signaling cascade in a strictly TβRI-dependent manner.
- The CD2AP-TβRI axis is identified as a promising novel prognostic biomarker and therapeutic target for HCC.

2.2. Data Acquisition and Processing

Transcriptomic data and corresponding clinical information for patients with HCC were obtained from The Cancer Genome Atlas (TCGA) and the Genotype-Tissue Expression (GTEx) project [35,36]. Expression data in HTSeq-FPKM format were normalized and converted to transcripts per million (TPM) values. For pan-cancer analysis, RNA-sequencing data in TPM format were additionally sourced from the UCSC Xena browser and the GTEx database [37].

2.3. Analysis of Differentially Expressed Genes (DEGs) and Functional Enrichment

Patients within the TCGA-HCC cohort were stratified into high and low CD2AP expression groups based on the median expression value. Differentially expressed genes (DEGs) between these groups were identified using the DESeq2 R package (v1.38.3) [38], with significance thresholds set at an adjusted p-value (padj) < 0.05 and an absolute log2 fold-change ($|\log_2 FC|$) > 1. Spearman's correlation analysis was performed to evaluate the relationship between CD2AP expression and that of the top 25 DEGs. Functional enrichment analysis of the identified DEGs, encompassing Gene Ontology (GO) terms and Kyoto Encyclopedia of Genes and Genomes (KEGG) pathways, was conducted using the GOplot R package (v1.0.2) [39].

2.4. Survival Analysis

Overall survival (OS), disease-specific survival (DSS), and progression-free interval (PFI) were analyzed using the Kaplan-Meier method, with statistical significance assessed by the log-rank test. The median expression level of CD2AP served as the cutoff for patient stratification. Univariate and multivariate Cox proportional-hazards regression models were employed to evaluate the prognostic value of clinicopathological variables. Variables yielding a p-value < 0.1

in univariate analysis were incorporated into the subsequent multivariate model. Hazard ratios and confidence intervals were visualized using forest plots generated with the ggplot2 R package.

2.5. Cell Culture

The human normal hepatocyte cell line WRL68 and a panel of human HCC cell lines (Huh-7, HEP3B2, Li-7, SNU-387, HepG2) were acquired from the Institute of Basic Medical Sciences, Chinese Academy of Medical Sciences. All cell lines were maintained at 37°C in a humidified incubator with 5% CO_2. Cells were cultured in RPMI-1640 medium (Gibco) supplemented with 10% (v/v) fetal bovine serum (FBS) and 1% (v/v) penicillin-streptomycin (100 U/mL penicillin and 100 μg/mL streptomycin). Cells were used for experiments between passages 5 and 10 to ensure phenotypic stability.

2.6. Generation of Genetically Modified Cell Lines

To generate CD2AP knockdown models, three independent small interfering RNAs targeting human CD2AP (siCD2AP-1, -2, -3; RiboBio) and a non-targeting control siRNA (siNC) were transfected into HepG2 cells using Lipofectamine 3000 reagent (Invitrogen) according to the manufacturer's protocol. The sense sequences of the three CD2AP-targeting siRNAs were: siCD2AP-1: 5'-AAGGCATGGGAATGTAGCAAGTCTT-3', siCD2AP-2: 5'-GAAGACCAAGAAGCGTCAGTGTAAA-3', siCD2AP-3: 5'-CAAGAAGCGTCAGTGTAAAGTTCTT-3'. HepG2 cells were selected for knockdown because preliminary western blot analysis indicated high endogenous CD2AP protein expression. Knockdown efficiency for each siRNA was evaluated by western blot, and siCD2AP-1, which produced the largest reduction in CD2AP, was chosen for subsequent in vitro functional assays.

For stable knockdown, a short hairpin RNA targeting CD2AP (shCD2AP), designed with the same validated targeting sequence as siCD2AP-1, and a non-targeting control shRNA (shControl) were cloned into lentiviral vectors (GeneChem). HepG2 cells were infected with the lentivirus and selected with puromycin to establish stable cell lines with sustained CD2AP knockdown, and interference efficiency was confirmed by western blot.

For CD2AP overexpression, a human CD2AP cDNA expression plasmid (GeneChem) or an empty vector control was transfected into LI-7 cells using the same transfection reagent for in vitro transient assays. LI-7 cells were selected because they exhibit low baseline CD2AP expression. For in vivo studies, a stable CD2AP-overexpressing LI-7 cell line and the corresponding empty vector control line were generated by lentiviral transduction followed by puromycin selection, and overexpression efficiency was verified by Western blot.

2.7. Cell Viability Assay

Cell viability was determined using a Cell Counting Kit-8 (CCK-8; Sevenbio) according to the manufacturer's instructions. Briefly, cells were seeded in 96-well plates at a density of 4×10^3 cells per well in 100 μL of complete medium. After incubation for 24, 48, 72, and 96 hours, 10 μL of CCK-8 reagent was added to each well. Plates were incubated at 37°C for 2 hours, and the absorbance at 450 nm was measured using a microplate reader.

2.8. Wound Healing and Transwell Assays

For the wound healing assay, HCC cells were seeded in 6-well plates (1×10^5cells per well) and cultured to approximately 90% confluence. A uniform linear wound was created in the monolayer using a sterile 200 μL pipette tip. The detached cells were removed by gently washing

twice with phosphate-buffered saline (PBS), and fresh serum-free medium was added. Wound images were captured at 0 and 24 hours post-scratching using an inverted microscope. The migration distance was quantified by measuring the wound width at three predetermined points per field using Axio Vision Rel. 4.8 software, and the relative migration rate was calculated. Experiments were performed in triplicate.

Cell invasion was assessed using a 24-well Transwell chamber system (Corning) with an 8.0 μm pore size polycarbonate membrane. The upper chamber membrane was pre-coated with 100 μL of Matrigel (diluted 1:8 in serum-free medium) and allowed to solidify at 37°C for 2 hours. HCC cells were harvested and resuspended in serum-free medium at a density of 1×10^5cells per 200 μL. This cell suspension was added to the upper chamber. The lower chamber was filled with 600 μL of complete medium containing 10% FBS as a chemoattractant. After 24 hours of incubation, non-invading cells on the upper surface of the membrane were carefully removed with a cotton swab. Cells that had invaded to the lower surface were fixed with 4% paraformaldehyde for 15 minutes, stained with 0.1% crystal violet for 20 minutes, and washed with PBS. Invading cells were imaged and counted in six randomly selected fields per well under a light microscope (200× magnification).

2.9. Western Blot and Co-Immunoprecipitation (Co-IP) Analysis

Total protein was extracted from cultured cells or snap-frozen tissue samples using RIPA lysis buffer supplemented with protease and phosphatase inhibitor cocktails. For tissues, samples were first homogenized on ice. Lysates were incubated on ice for 30 minutes and then centrifuged at 12,000 × g for 10 minutes at 4°C. The supernatant was collected, and protein concentration was determined using a bicinchoninic acid (BCA) assay kit. Equal amounts of

protein (20-40 μg) were mixed with 5× SDS loading buffer, denatured by boiling at 95°C for 10 minutes, and separated by electrophoresis on 8-12% SDS-polyacrylamide gels. Proteins were subsequently transferred onto 0.45 μm polyvinylidene difluoride (PVDF) membranes using a wet transfer system at a constant current of 300 mA for 60-90 minutes. Membranes were blocked with 5% bovine serum albumin (BSA) in Tris-buffered saline containing 0.1% Tween-20 (TBST) for 1 hour at room temperature, followed by incubation with primary antibodies diluted in blocking buffer overnight at 4°C. After three washes with TBST (10 minutes each), membranes were incubated with horseradish peroxidase (HRP)-conjugated secondary antibodies for 1 hour at room temperature. Following another three TBST washes, protein bands were visualized using an enhanced chemiluminescence (ECL) substrate and imaged with a CLINX 6100 chemiluminescence detection system.

For Co-IP, cell lysates (500-1000 μg of total protein) were pre-cleared with Protein A/G Magnetic Beads for 1 hour at 4°C. The pre-cleared lysates were then incubated with 2-4 μg of the indicated primary antibody or control IgG overnight at 4°C with gentle rotation. Protein A/G Magnetic Beads were added and incubated for an additional 2-4 hours. The bead-bound immunocomplexes were washed five times with ice-cold lysis buffer, eluted by boiling in 2× SDS loading buffer, and analyzed by western blotting as described above.

The following primary antibodies were used: CD2AP (Invitrogen, PA5-51894, 1:600), TGF-β1 (Abcam, ab215715, 1:1000), Smad3 (Abcam, ab40854, 1:1000), phospho-Smad3 (Ser423/425; Abcam, ab52903, 1:2000), E-cadherin (Abcam, ab314063, 1:1000), N-cadherin (Abcam, ab76011, 1:5000), Vimentin (Abcam, ab8978, 1:1000), Zonula Occludens-1 (ZO-1) (Abcam, ab221547, 1:1000). HRP-conjugated secondary antibodies (Abcam, ab205722, 1:5000) were used for detection.

2.10. Immunofluorescence (IF) Staining

Cells grown on sterile glass coverslips in 24-well plates were fixed with 4% paraformaldehyde for 15 minutes at room temperature, permeabilized with 0.5% Triton X-100 in PBS for 10 minutes, and blocked with 5% BSA for 1 hour. The cells were then incubated overnight at 4°C with primary antibodies against ZO-1 (1:200) and Vimentin (1:600) diluted in blocking buffer. After three washes with PBS, cells were incubated with Alexa Fluor 594-conjugated secondary antibodies (Beyotime, 1:800) for 1 hour at room temperature in the dark. Nuclei were counterstained with DAPI (Biosharp, 1:1000) for 5 minutes. Following final washes, coverslips were mounted onto glass slides with anti-fade mounting medium. Fluorescence images were acquired using a fluorescence microscope within 4 hours and processed with ImageJ software.

2.11. Protein-Protein Docking

The three-dimensional structures of human CD2AP (UniProt ID: Q9Y5K6) and TGF-β Receptor I (TβRI; UniProt ID: P36897) were retrieved from the UniProt database [40]. The crystal structure of CD2AP (PDB ID: 4WCI) was defined as the ligand, and the structure of TβRI (PDB ID: 5E8S) was defined as the receptor for docking studies. Global protein-protein docking was performed using the HDOCKlite v1.1 server [41], which employs a hybrid scoring function combining physics-based and template-based potentials to systematically sample rotational and translational space. The server generated 100 potential binding poses. Docking results were evaluated based on the HDOCK score (where more negative values indicate higher predicted binding affinity) and a confidence score (where values >0.7, 0.5–0.7, and <0.5 denote high, medium, and low reliability of the model, respectively).

2.12. Molecular Dynamics (MD) Simulation

Molecular dynamics simulations were performed using GROMACS 2022.4 [42] to assess the stability of the predicted CD2AP-TβRI complex. The AMBER14SB force field was applied to the proteins, and ligand parameters were generated using the GAFF2 force field via the ACPYPE server. The complex was solvated in a cubic box of TIP3P water molecules with a minimum distance of 1.0 nm between the solute and box edge. The system was neutralized with Na^+/Cl^- ions and brought to a physiological concentration of 0.15 M NaCl. Energy minimization was conducted using the steepest descent algorithm until a maximum force below 1000 kJ/mol/nm was reached. Subsequently, the system was equilibrated in two phases: a 100 ps NVT (constant Number of particles, Volume, and Temperature) simulation at 310 K using the V-rescale thermostat, followed by a 100 ps NPT (constant Number of particles, Pressure, and Temperature) simulation at 1 bar using the Parrinello-Rahman barostat. Long-range electrostatic interactions were calculated using the Particle Mesh Ewald (PME) method with a 1.0 nm cutoff. Bond lengths were constrained using the LINCS algorithm. Finally, a 100 ns production MD simulation was performed in the NPT ensemble. Trajectory analysis included calculations of root-mean-square deviation (RMSD), root-mean-square fluctuation (RMSF), the number of hydrogen bonds, radius of gyration (Rg), and solvent-accessible surface area (SASA) using built-in GROMACS tools.

2.13 Mouse Xenograft Models

All animal procedures were approved by the Laboratory Animal Ethics Committee of Xinjiang Medical University (Approval No. XJMU-IACUC-20260123-04) and performed in strict accordance with institutional guidelines for the care and use of laboratory animals. Four-to-

five-week-old female BALB/c nude mice (specific pathogen-free grade) were maintained under controlled specific pathogen-free conditions (temperature: 23 ± 2° C; humidity: 55 ± 5%) on a 12-hour light/dark cycle with ad libitum access to sterilized food and water. To establish subcutaneous xenografts, HepG2 cells stably expressing shCD2AP or shControl and LI-7 cells stably overexpressing CD2AP or empty vector were harvested in the logarithmic growth phase. Cell viability exceeded 95% as assessed by Trypan Blue exclusion. A single-cell suspension of 4 × 10^5 cells in 100 μL sterile phosphate-buffered saline (PBS) was injected subcutaneously into the right flank of each anesthetized mouse (n = 6 per group). Tumor growth was measured every three days by recording the maximum length (L) and minimum width (W) with a digital caliper. Tumor volume was calculated using the formula Volume = (L × W^2) / 2. Mice were euthanized by cervical dislocation 28 days after inoculation, and subcutaneous tumors were excised, weighed, and either snap-frozen in liquid nitrogen for protein analysis or fixed in 4% paraformaldehyde for histopathology.

2.14. In Vivo Imaging System (IVIS)

For in vivo imaging, HepG2 cells stably expressing both shCD2AP/shControl and a luciferase reporter gene were used to generate xenografts. Tumor growth was monitored weekly using an IVIS Spectrum in vivo imaging system (PerkinElmer). Mice were anesthetized with 2% isoflurane and injected intraperitoneally with D-luciferin potassium salt (150 mg/kg body weight; GoldBio). Bioluminescence images were acquired 10 minutes post-injection with an exposure time of 1-60 seconds (auto-scaled). Total flux (photons/second) within a defined region of interest (ROI) covering the tumor signal was quantified using Living Image 4.7.1 software (PerkinElmer).

3. RESULTS

3.1 Elevated Expression of CD2AP in HCC

Bioinformatic analysis across multiple cancer types revealed that CD2AP is frequently overexpressed, including in esophageal carcinoma, glioblastoma multiforme, liver hepatocellular carcinoma (LIHC), lung adenocarcinoma, and stomach adenocarcinoma (Fig. 1A). Consistent with this pan-cancer pattern, CD2AP mRNA levels were significantly elevated in HCC tumor samples compared to normal liver tissues in the TCGA cohort (p <0.001) (Fig. 1B). This overexpression was further validated in 110 matched tumor-normal pairs, where CD2AP expression was markedly higher in the HCC tissues (p <0.001) (Fig. 1C). To evaluate the diagnostic potential of CD2AP, a receiver operating characteristic (ROC) curve was constructed. The analysis yielded an area under the curve (AUC) of 0.803 (95% CI: 0.758–0.847), indicating robust discriminative power for distinguishing HCC from normal liver tissue (Fig. 1D).

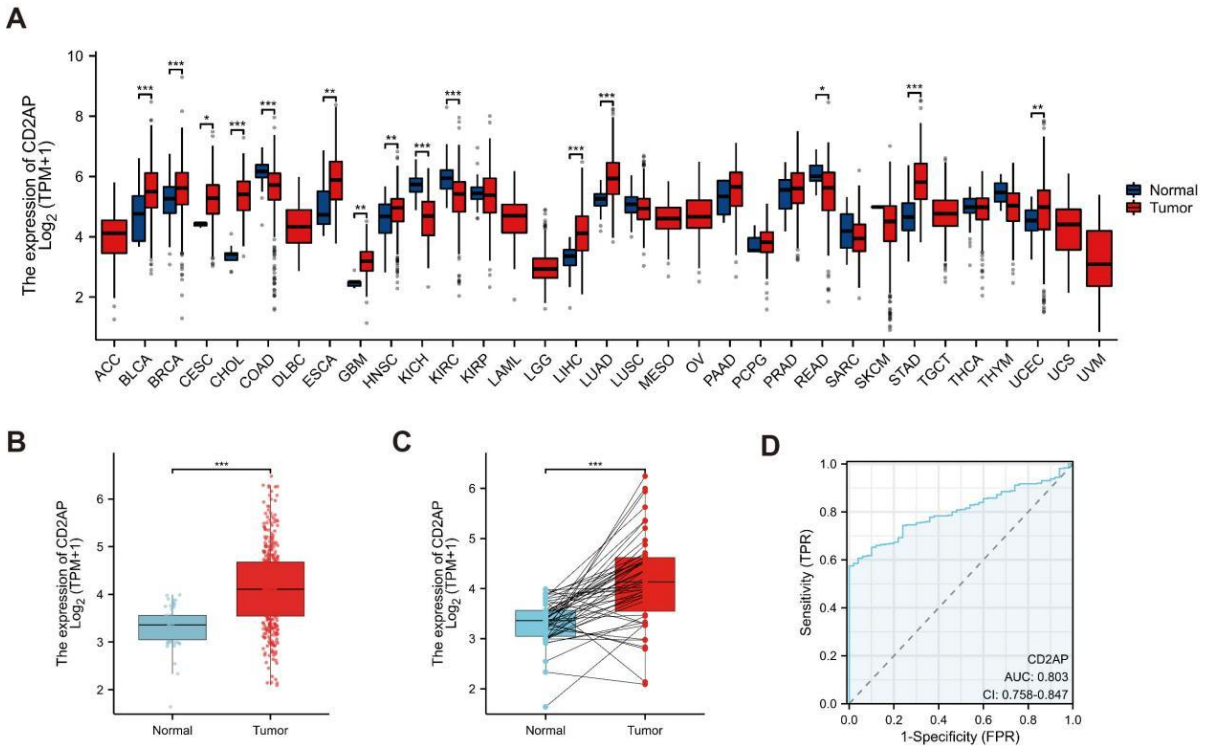


Fig. 1: CD2AP is overexpressed in human cancers and demonstrates diagnostic potential in hepatocellular carcinoma. (A) Pan-cancer analysis of CD2AP mRNA expression across tumor types and corresponding normal tissues from TCGA and GTEx databases. (B) CD2AP expression is significantly upregulated in unpaired HCC tissues compared to normal liver tissues in the TCGA cohort. (C) Validation of CD2AP overexpression in paired tumor and adjacent non-tumor tissues from HCC patients in TCGA. (D) Receiver operating characteristic (ROC) curve evaluating the diagnostic performance of CD2AP for discriminating HCC from normal liver tissue. TCGA, The Cancer Genome Atlas; GTEx, Genotype-Tissue Expression project. ***p <0.001.

3.2. Associations Between CD2AP Expression and Clinicopathologic Variables

High expression of CD2AP demonstrated significant correlations with key clinicopathological indicators of more advanced disease. As summarized in Table 1, elevated CD2AP levels were significantly associated with higher pathologic stage (p =0.049), positive tumor status (p =0.027), increased patient weight (p =0.022), and poorer histologic grade (p <0.001). Conversely, CD2AP expression showed no statistically significant association with patient age, individual T/N/M stages, gender, or histological subtype (all p >0.05).

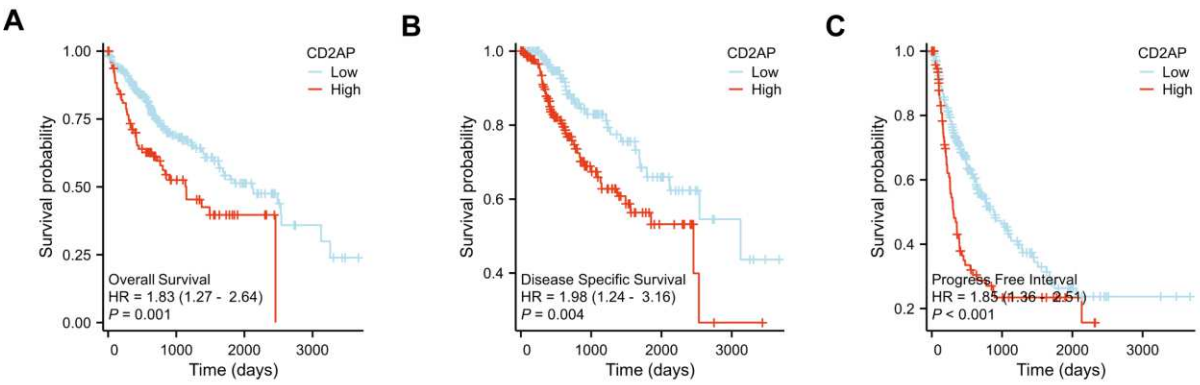
Tab. 1 Clinicopathological characteristics of high- and low-CD2APexpression groups.

Characteristics	Low expression of CD2AP	High expression of CD2AP	P value
n	187	187	
Age, n (%)			0.109
<= 60	81 (21.7%)	96 (25.7%)	
> 60	106 (28.4%)	90 (24.1%)	
Pathologic T stage, n (%)			0.078
T1	103 (27.8%)	80 (21.6%)	
T2	39 (10.5%)	56 (15.1%)	
T3	36 (9.7%)	44 (11.9%)	
T4	7 (1.9%)	6 (1.6%)	
Pathologic N stage, n (%)			0.636
N0	126 (48.8%)	128 (49.6%)	
N1	1 (0.4%)	3 (1.2%)	
Pathologic M stage, n (%)			0.583
M0	130 (47.8%)	138 (50.7%)	
M1	3 (1.1%)	1 (0.4%)	
Pathologic stage, n (%)			0.049

Characteristics	Low expression of CD2AP	High expression of CD2AP	P value
Stage I	96 (27.4%)	77 (22%)	
Stage II	38 (10.9%)	49 (14%)	
Stage III	35 (10%)	50 (14.3%)	
Stage IV	4 (1.1%)	1 (0.3%)	
Tumor status, n (%)			0.027
Tumor free	111 (31.3%)	91 (25.6%)	
With tumor	66 (18.6%)	87 (24.5%)	
Gender, n (%)			0.740
Female	59 (15.8%)	62 (16.6%)	
Male	128 (34.2%)	125 (33.4%)	
Histological type, n (%)			0.443
Fibrolamellar carcinoma	2 (0.5%)	1 (0.3%)	
Hepatocellular carcinoma	183 (48.9%)	181 (48.4%)	
Hepatocholangiocarcinoma (mixed)	2 (0.5%)	5 (1.3%)	
Weight, n (%)			0.022
<= 70	83 (24%)	101 (29.2%)	
> 70	93 (26.9%)	69 (19.9%)	
Histologic grade, n (%)			< 0.001
G1	38 (10.3%)	17 (4.6%)	
G2	96 (26%)	82 (22.2%)	
G3	48 (13%)	76 (20.6%)	
G4	4 (1.1%)	8 (2.2%)	

3.3. Prognostic Value of CD2AP in HCC

To assess the prognostic relevance of CD2AP, patients with HCC were stratified into high- and low-expression groups based on the median expression level. Kaplan-Meier survival analysis revealed that elevated CD2AP expression was significantly associated with poorer clinical outcomes. Compared to the low-expression group, patients with high CD2AP expression exhibited significantly shorter overall survival (OS; HR = 1.83, 95% CI: 1.27–2.64, p =0.001), disease-specific survival (DSS; HR = 1.98, 95% CI: 1.24–3.16, p =0.004), and progression-free interval (PFI; HR = 1.85, 95% CI: 1.36–2.51, p <0.001) (Fig. 2A–C). Furthermore, multivariate Cox regression analysis identified high CD2AP expression as an independent prognostic factor for OS, along with pathologic stage and T stage (Fig. 2D).



D

Characteristics	Total(N)	HR(95% CI)	P value
Age	373		
<= 60	177	Reference	
> 60	196	0.960 (0.718 - 1.284)	0.783
Gender	373		
Female	121	Reference	
Male	252	0.982 (0.721 - 1.338)	0.909
Histologic grade	368		
G1	55	Reference	
G2	178	1.167 (0.750 - 1.814)	0.494
G3	123	1.313 (0.832 - 2.071)	0.242
G4	12	1.082 (0.415 - 2.823)	0.872
Pathologic stage	349		
Stage I	173	Reference	
Stage II	86	1.905 (1.305 - 2.780)	< 0.001
Stage III	85	2.678 (1.857 - 3.861)	< 0.001
Stage IV	5	5.576 (1.728 - 17.992)	0.004
Pathologic T stage	370		
T1	183	Reference	
T2	94	2.020 (1.411 - 2.892)	< 0.001
T3	80	2.620 (1.811 - 3.789)	< 0.001
T4	13	4.266 (2.181 - 8.347)	< 0.001
Pathologic N stage	258		
N0	254	Reference	
N1	4	1.370 (0.338 - 5.552)	0.659
Pathologic M stage	272		
M0	268	Reference	
M1	4	3.476 (1.091 - 11.076)	0.035

Fig. 2: High CD2AP expression predicts poor survival outcomes in hepatocellular carcinoma. (A–C) Kaplan-Meier survival curves demonstrate that patients with high CD2AP expression exhibit significantly worse (A) overall survival (OS), (B) disease-specific survival (DSS), and (C) progression-free interval (PFI) compared to those with low expression. (D) Forest plot from multivariate Cox regression analysis identifies high CD2AP expression as an independent prognostic factor for shorter OS.

3.4. Identification of DEGs in HCC and Functional Enrichment Analysis Including GO, KEGG

Differential expression analysis identified 4,632 genes significantly dysregulated between CD2AP-high and CD2AP-low HCC groups (adjusted p-value < 0.05, $|\log_2 FC| > 1$), comprising 2,853 upregulated and 1,779 downregulated genes (Fig. 3A). A strong correlation was observed between CD2AP expression and the top 25 most significantly associated DEGs (e.g., LHFPL3-AS2, TMEM256, HP, NCEH1) (Fig. 3B).Gene Ontology (GO) enrichment analysis revealed that the DEGs were significantly enriched in biological processes related to tissue morphogenesis, pattern specification, and mesenchyme development. Cellular component terms included side of membrane and microtubule-associated complex, while molecular functions involved active transmembrane transporter activity, phosphatase binding, and carboxylic acid binding (Fig. 3C). Kyoto Encyclopedia of Genes and Genomes (KEGG) pathway analysis further demonstrated significant enrichment in key oncogenic pathways, including the Epithelial-mesenchymal transition, TGF-beta signaling pathway, Adherens junction, and Neutrophil extracellular trap formation (Fig. 3D).

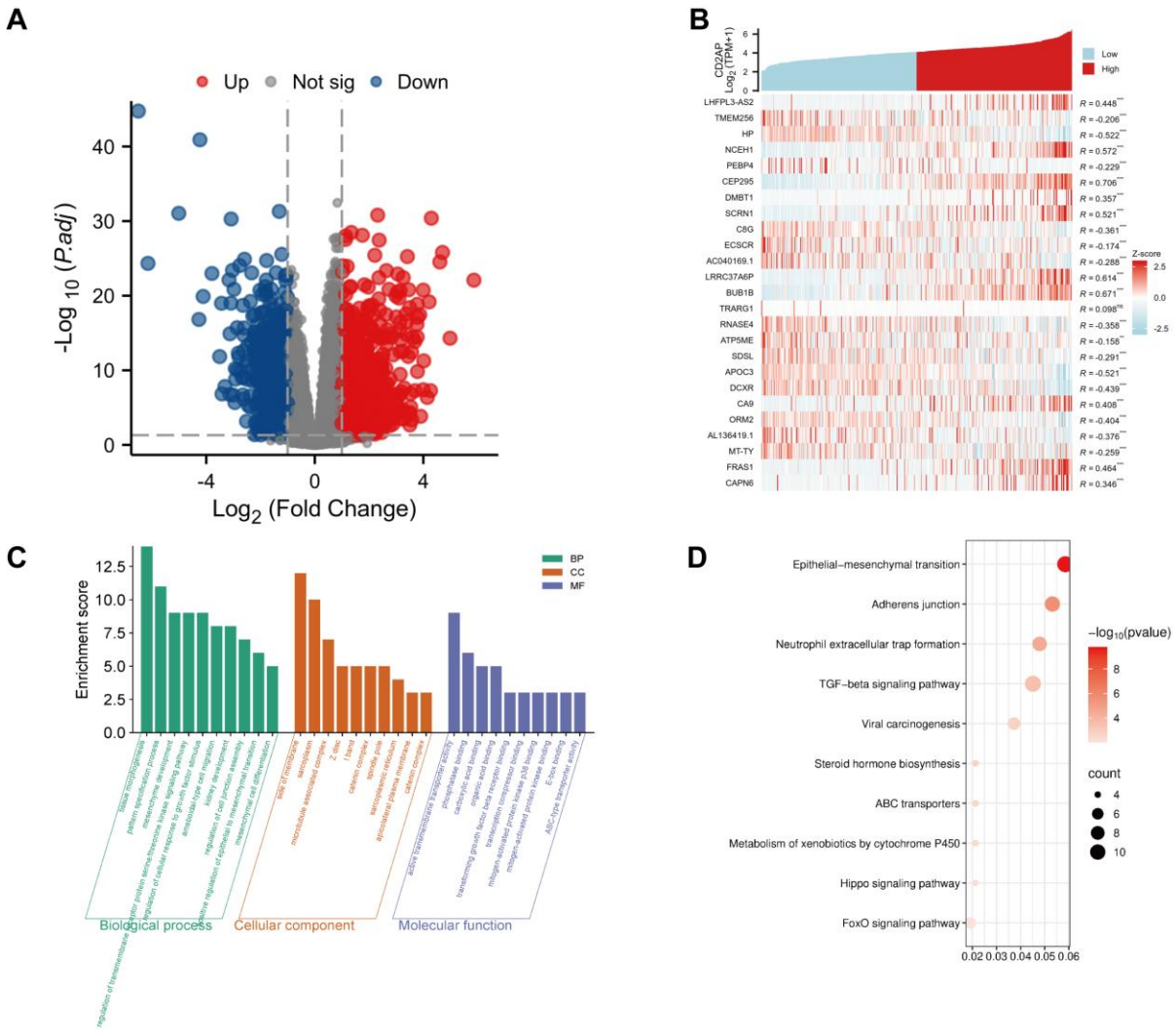


Fig. 3: Functional enrichment of CD2AP-correlated genes implicates EMT and TGF-β signaling in HCC progression. (A) Volcano plot depicting 4,632 differentially expressed genes (DEGs) associated with high versus low CD2AP expression. Red and blue dots denote significantly upregulated and downregulated genes, respectively ($|\log_2 FC| > 1$, adj. $p < 0.05$). (B) Heatmap illustrating the strong co-expression pattern between CD2AP and the top 25 most significantly correlated DEGs. (C) Gene Ontology (GO) enrichment analysis of DEGs across biological process, cellular component, and molecular function categories. (D) Kyoto Encyclopedia of Genes and Genomes (KEGG) pathway enrichment analysis highlights significant involvement in epithelial-mesenchymal transition and TGF-β signaling.

3.5. CD2AP regulates HCC cell proliferation, migration, and invasion

To investigate the functional role of CD2AP in hepatocellular carcinoma, we first analyzed its endogenous protein expression across a panel of cell lines. Western blotting revealed that CD2AP expression was highest in HepG2 cells and lowest in LI-7 cells among the HCC lines examined (Fig. 4A). Based on this screening, HepG2 and LI-7 cells were selected for loss-of-function and gain-of-function studies, respectively. Transfection of HepG2 cells with three independent siRNAs targeting CD2AP identified siCD2AP-1 as the most efficient, as confirmed by western blot analysis (Fig. 4B). Knockdown of CD2AP using siCD2AP-1 significantly impaired HepG2 cell proliferation (Fig. 4C), migration (Fig. 4D), and invasion (Fig. 4E). Conversely, stable overexpression of CD2AP in LI-7 cells (Fig. 4F) markedly enhanced these malignant phenotypes, including proliferation (Fig. 4H), migration (Fig. 4G), and invasion (Fig. 4I). Taken together, these findings demonstrate that CD2AP functionally drives the proliferative, migratory, and invasive capacities of HCC cells.

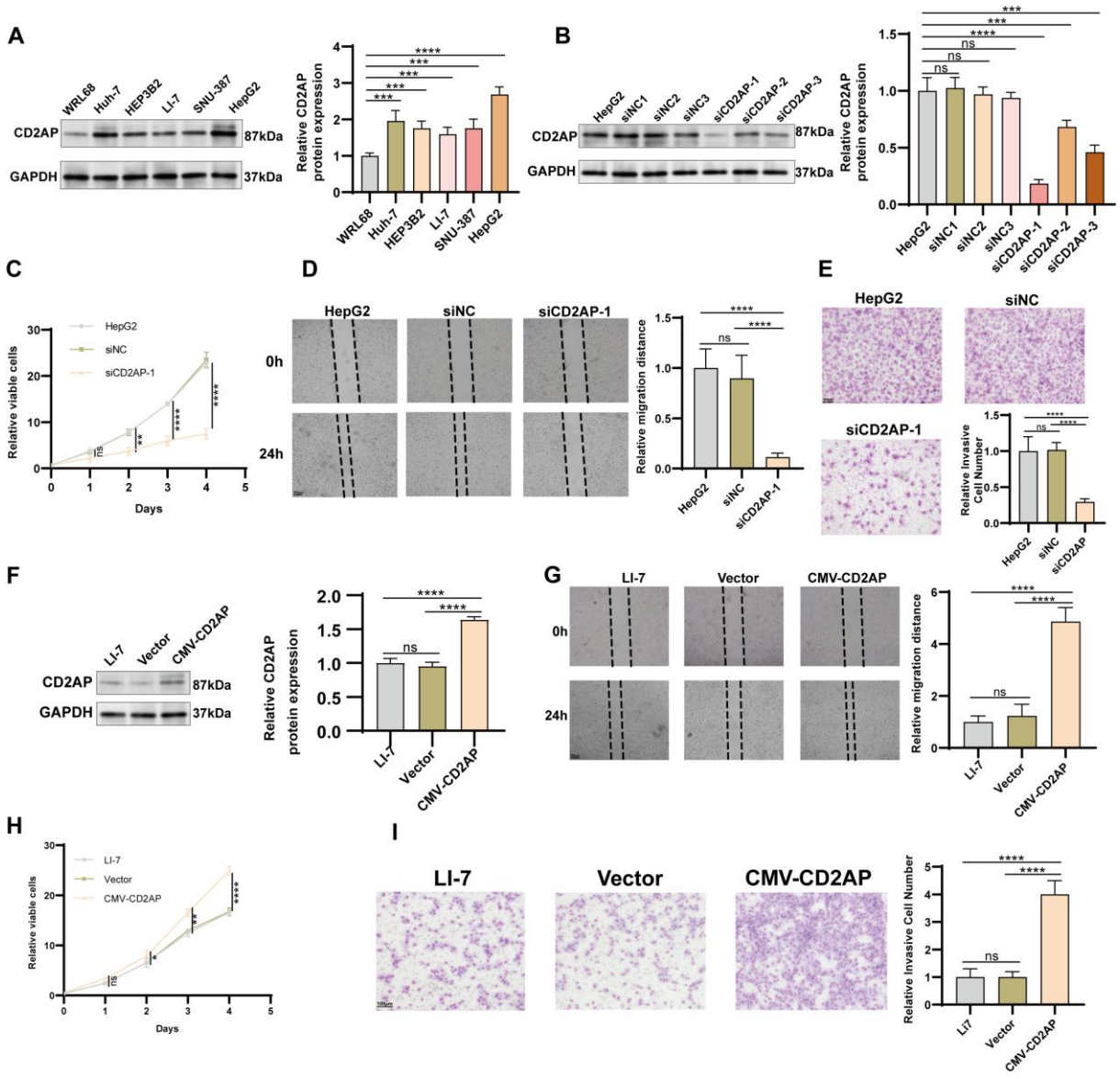


Fig. 4: CD2AP is essential for the malignant phenotype of HCC cells in vitro. (A) Endogenous CD2AP protein expression in a panel of HCC cell lines, with HepG2 showing the highest and LI-7 the lowest level. (B) Validation of siRNA-mediated CD2AP knockdown in HepG2 cells; siCD2AP-1 was selected for subsequent functional assays. (C–E) Depletion of CD2AP significantly attenuated the (C) proliferative, (D) migratory, and (E) invasive capacities of HepG2 cells. (F) Ectopic overexpression of CD2AP in LI-7 cells. (G–I) Conversely, CD2AP overexpression markedly enhanced (G) cell migration, (H) proliferation, and (I) invasion in LI-7 cells. Data are presented as mean ± SD. ns, not significant; *$p < 0.05$, **$p < 0.01$, ***$p < 0.001$, ****$p < 0.0001$.

3.6. CD2AP Activates the TGF-β1/Smad3 Pathway and Drives EMT in HCC Cells

To determine whether CD2AP regulates epithelial-mesenchymal transition (EMT) and the TGF-β1/Smad3 signaling axis in HCC, we assessed key molecular markers following genetic manipulation of CD2AP. In HepG2 cells, siRNA-mediated knockdown of CD2AP led to a significant increase in epithelial markers (E-cadherin and ZO-1) and a concomitant decrease in mesenchymal markers (Vimentin and N-cadherin) (Fig. 5A). This was accompanied by a suppression of the TGF-β1/Smad3 pathway, as demonstrated by reduced protein levels of TβRI and phospho-Smad3 (p-Smad3) (Fig. 5B). Conversely, in LI-7 cells, ectopic overexpression of CD2AP induced a pronounced EMT, characterized by downregulation of E-cadherin and ZO-1 and upregulation of Vimentin and N-cadherin (Fig. 5C). Consistent with this shift, CD2AP overexpression potentiated TGF-β1 signaling, elevating the levels of TβRI and p-Smad3 (Fig. 5D). Notably, neither silencing nor overexpression of CD2AP altered the total protein level of TGF-β1 ligand and total Smad3, while the protein abundance of TβRI, phosphorylation level of Smad3, and EMT phenotype were significantly modulated by CD2AP expression. These results indicate that CD2AP positively regulates the downstream TGF-β1/Smad3 signaling pathway activity and EMT phenotype via TβRI, acting downstream of TGF-β1 ligand production, at the level of TβRI receptor.

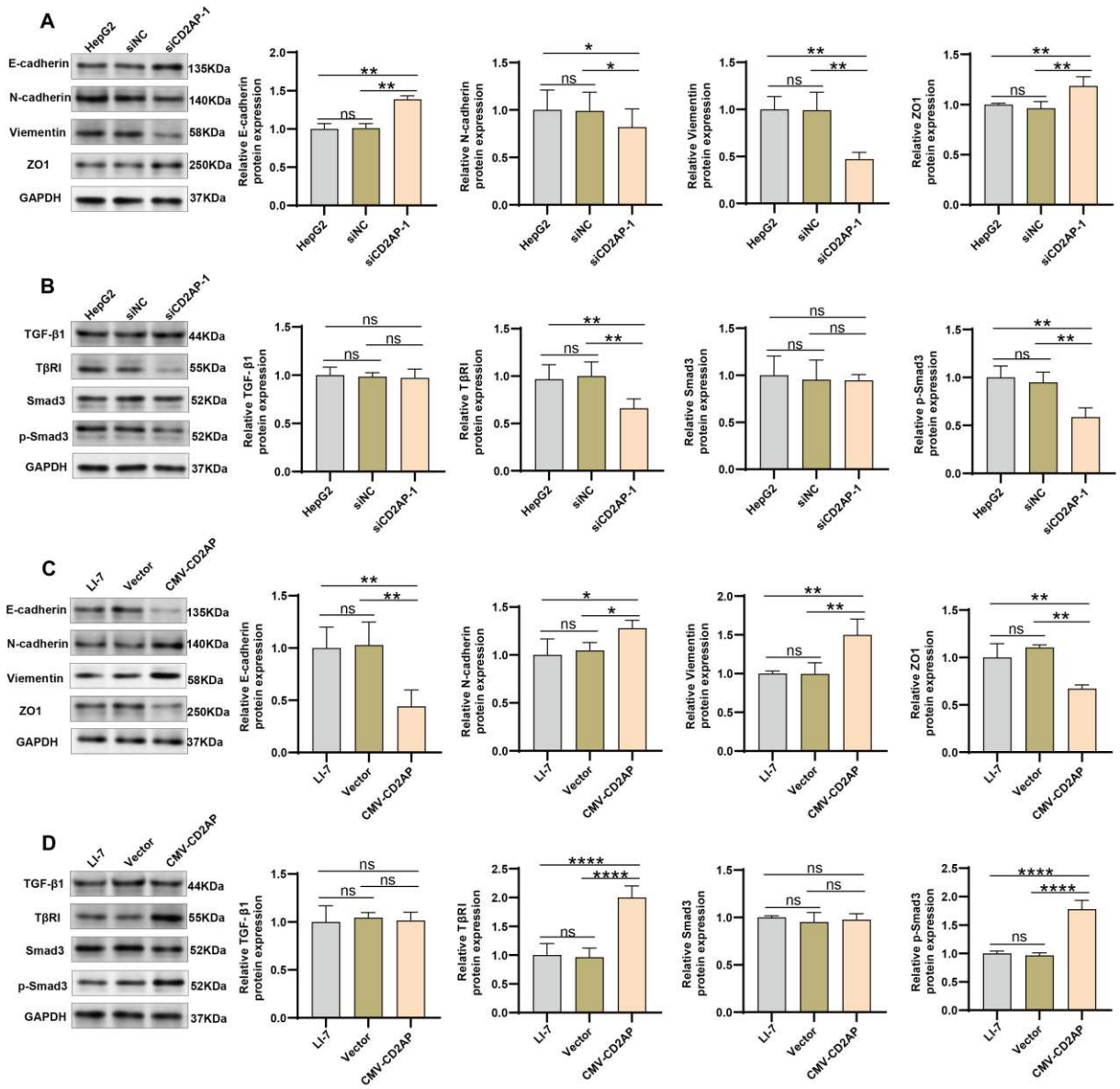


Fig. 5: CD2AP drives EMT and activates the TGF-β1/Smad3 pathway in HCC cells. (A, B) In HepG2 cells, CD2AP knockdown reversed the EMT phenotype, increasing epithelial markers (E-cadherin, ZO-1) and decreasing mesenchymal markers (Vimentin, N-cadherin) (A), while concurrently suppressing the TGF-β1/Smad3 pathway, as shown by reduced TβRI and p-Smad3 levels (B). (C, D) Conversely, in LI-7 cells, CD2AP overexpression induced EMT, downregulating epithelial markers and upregulating mesenchymal markers (C), and potentiated TGF-β1 signaling, evidenced by increased TβRI and p-Smad3 (D). Notably, TGF-β1 and total Smad3 levels remained unchanged upon CD2AP modulation. Data are presented as mean ± SD. ns, not significant; *$p < 0.05$, **$p < 0.01$, ***$p < 0.001$, ****$p < 0.0001$.

3.7. Immunofluorescence Validates CD2AP-Dependent Regulation of EMT Markers

Immunofluorescence analysis corroborated the western blot findings. CD2AP knockdown in HepG2 cells substantially diminished Vimentin signal (Fig. 6A) and intensified ZO-1 staining (Fig. 6B). In contrast, CD2AP overexpression in LI-7 cells markedly enhanced Vimentin fluorescence (Fig. 6C) while attenuating ZO-1 expression (Fig. 6D), providing visual confirmation of CD2AP's role in promoting a mesenchymal phenotype.

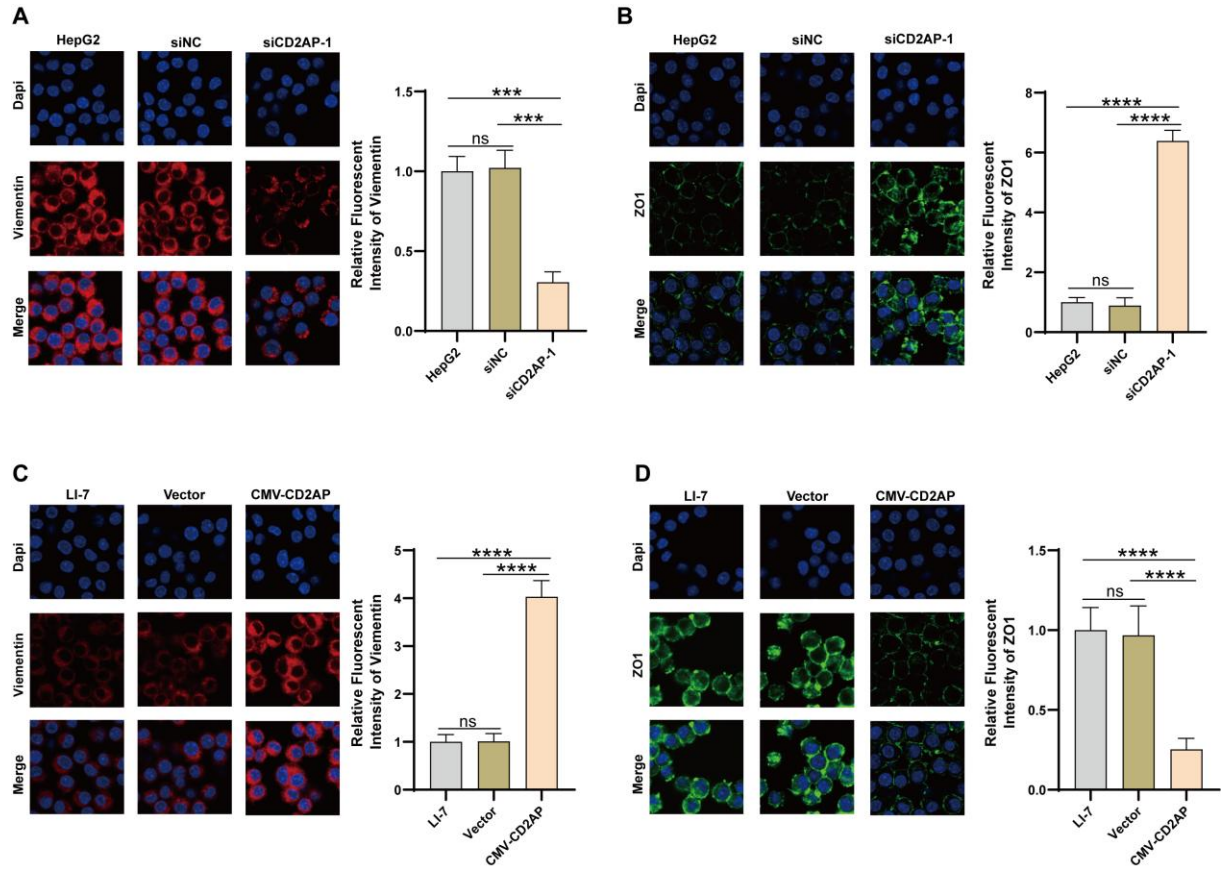


Fig. 6: CD2AP modulates EMT markers in HCC cells. (A) Immunofluorescence analysis of Vimentin expression in HepG2 cells following CD2AP knockdown. (B) Immunofluorescence staining of the tight junction protein ZO1 in HepG2 cells after CD2AP knockdown. (C) Vimentin expression in LI-7 cells upon CD2AP overexpression. (D) ZO1 expression in LI-7 cells following CD2AP overexpression. Data are presented as mean ± SD. ns, not significant; *$p < 0.05$, **$p < 0.01$, ***$p < 0.001$, ****$p < 0.0001$.

3.8. CD2AP-TβRI Interaction and Complex Structural Stability

The interaction between CD2AP and TβRI was investigated using integrated experimental and computational approaches. Endogenous Co-IP in HCC cells confirmed a physical interaction between CD2AP and TβRI (Fig. 7A). To characterize this complex structurally, molecular docking was performed, yielding a top-ranked model (model_1) with a high-affinity binding energy of −242.95 kcal/mol and a confidence score of 0.8652, indicating a high probability of complex formation (Fig. 7B). Surface representation of the model delineated a well-defined binding interface (Fig. 7C). Analysis of the interface with the Protein–Ligand Interaction Profiler (PLIP) identified key stabilizing interactions, including hydrogen bonds (e.g., TβRI-Arg240 with CD2AP-Val29; TβRI-Ser241 with CD2AP-Asn28) and a salt bridge (TβRI-Arg237 with CD2AP-Glu39) (Fig. 7D).

To assess the dynamic stability of the complex, a 100-ns molecular dynamics (MD) simulation was conducted. The root-mean-square deviation (RMSD) plateaued at approximately 2.1 Å after 60 ns, indicating convergence to a stable conformational state (Fig. 7F). Minor fluctuations in the radius of gyration (Rg) and solvent-accessible surface area (SASA) suggested localized structural adjustments during the simulation (Fig. 7G, H). The free-energy landscape (FEL) plotted against RMSD and Rg revealed a low-energy basin (blue region), consistent with a thermodynamically favored conformation (Fig. 7E). The number of hydrogen bonds remained stable at two throughout the trajectory, supporting a persistent interaction network (Fig. 7I). Furthermore, root-mean-square fluctuation (RMSF) values for most residues remained below 4 Å, reflecting limited flexibility and overall structural rigidity of the complex (Fig. 7J, K). Collectively, these experimental and computational data demonstrate that CD2AP and TβRI form a stable, high-affinity complex in HCC.

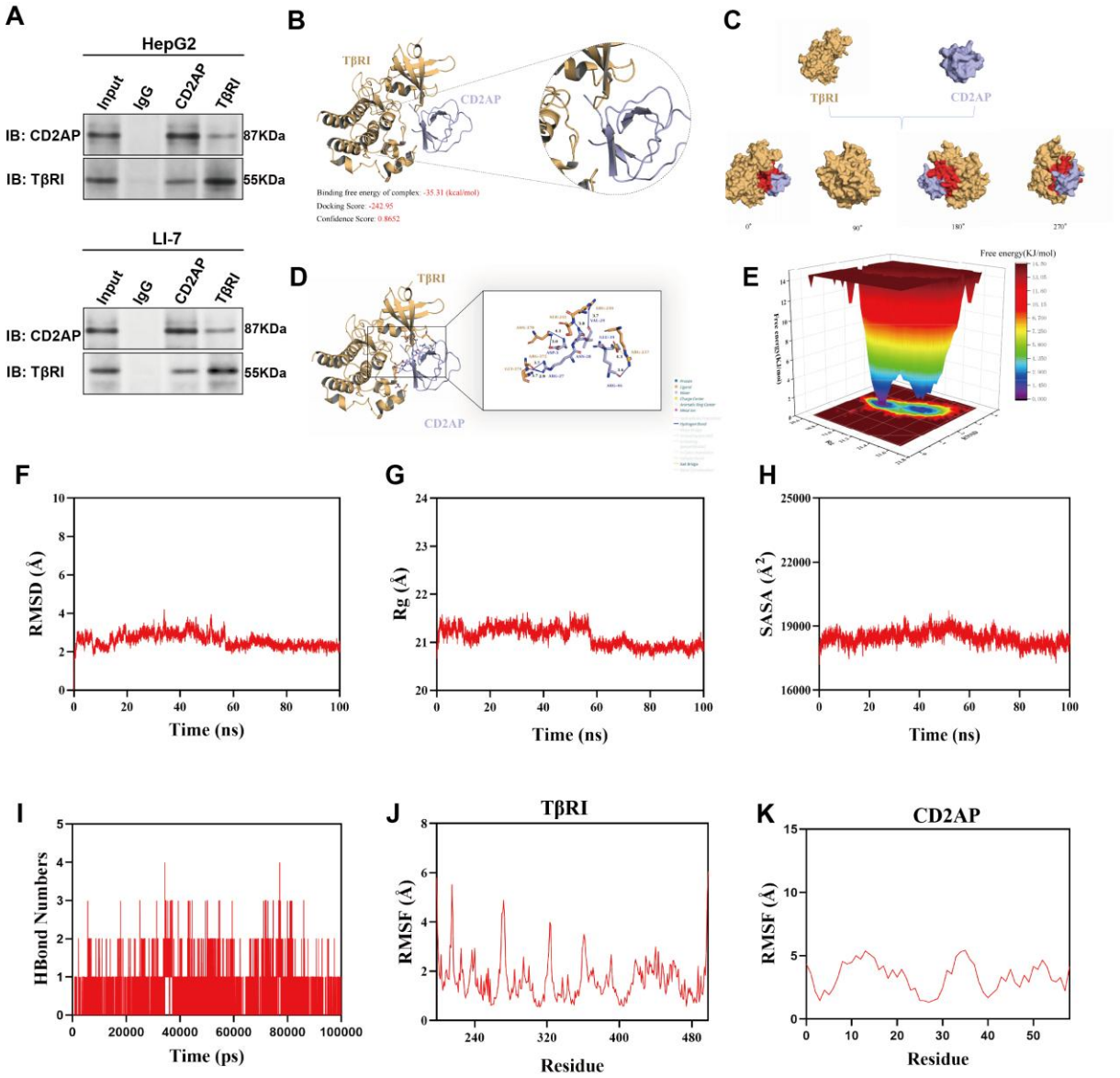


Fig. 7: Structural and biophysical characterization of the CD2AP–TβRI complex. (A) Endogenous Co-IP confirms the interaction between CD2AP and TβRI in HCC cells. (B) Top-ranked docking pose of the CD2AP (purple)–TβRI (yellow) complex, with a high-affinity binding score. (C) Surface representation highlighting the complementary binding interface (red) between the two proteins. (D) Atomic interaction map from PLIP analysis, detailing key hydrogen bonds and salt bridges stabilizing the complex. (E) Free-energy landscape (FEL) projected onto RMSD and Rg, identifying the lowest-energy conformational basin. (F–I) Time-evolution profiles of the complex during 100-ns MD simulations: (F) root-mean-square deviation (RMSD), (G) radius of gyration (Rg), (H) solvent-accessible surface area (SASA), and

(I) number of inter-protein hydrogen bonds. (J, K) Per-residue root-mean-square fluctuation (RMSF) for TβRI (J) and CD2AP (K), indicating regions of structural flexibility.

The combined Co-IP, molecular docking, and dynamics simulations confirm that CD2AP and TβRI can form a stable, high-affinity protein complex in HCC cells, which acts as the key molecular basis for CD2AP to positively regulate the TGF-β1/Smad3 signaling pathway via TβRI.To graphically summarize the proposed oncogenic axis, a schematic model is presented in Fig. 8.

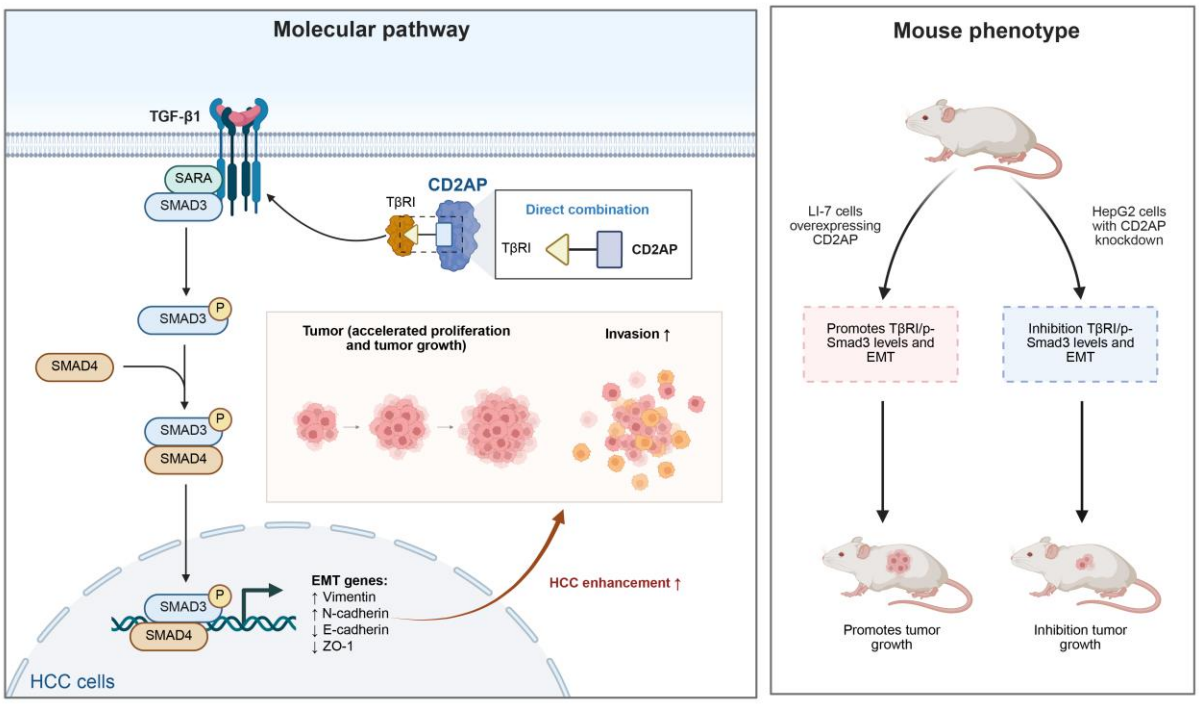


Fig. 8: Proposed model of the CD2AP–TβRI oncogenic axis driving EMT and HCC progression. Schematic summarizing the molecular mechanism through which CD2AP promotes hepatocellular carcinoma progression. CD2AP directly binds to and Positively Regulates TβRI at the cell membrane, potentiating TGF-β1-induced Smad3 phosphorylation. Phosphorylated Smad3 forms a complex with Smad4 and translocates to the nucleus, where it transcriptionally reprograms EMT-related genes—upregulating mesenchymal markers (Vimentin, N-cadherin) and downregulating epithelial markers (ZO-1, E-cadherin). This EMT switch enhances tumor cell proliferation, invasion, and metastasis, thereby accelerating HCC progression in vivo. The model integrates findings from loss- and gain-of-function studies in HCC cells and mouse

xenografts, confirming CD2AP as a critical upstream activator of the TGF-β1/Smad3-EMT axis.

3.9. CD2AP regulates migration, invasion and EMT progression of HCC cells in a TβRI-dependent manner

In HepG2 cells that express high endogenous CD2AP, gradient concentrations of TGF-β1 were applied to specifically activate TβRI, and functional rescue experiments were performed after CD2AP knockdown to clarify CD2AP's role in regulating malignant behaviours of HCC cells via TβRI. The wound-healing assay showed (Fig. 9A) that exogenous TGF-β1 significantly enhanced HepG2 cell migration in a concentration-dependent manner (0, 5, 10 ng/mL); the 24 h relative migration distance increased progressively as TGF-β1 concentration rose. CD2AP knockdown markedly inhibited the basal migratory ability of HepG2 cells, whereas supplementation with 20 ng/mL exogenous TGF-β1 significantly reversed this inhibitory effect on migration. The Transwell invasion assay (Fig. 9B) showed a consistent trend: gradient concentrations of TGF-β1 significantly increased the number of transmembrane invasive HepG2 cells in a concentration-dependent manner. CD2AP knockdown markedly suppressed HepG2 invasive capacity, and addition of 20 ng/mL exogenous TGF-β1 significantly reversed this suppression and restored invasiveness. Western blot analysis of core pathway proteins showed (Fig. 9C) that TGF-β1 treatment upregulated TβRI protein expression in HepG2 cells in a concentration-dependent manner and simultaneously increased phosphorylation of downstream Smad3. CD2AP knockdown markedly reduced basal TβRI protein levels and inhibited Smad3 phosphorylation and activation. Supplementation with 20 ng/mL exogenous TGF-β1 significantly reversed the CD2AP-knockdown–induced downregulation of TβRI and the inhibition of Smad3 phosphorylation, restoring activation of the TβRI/Smad3 signalling pathway. Detection of EMT markers showed (Fig. 9D) that TGF-β1 treatment downregulated the epithelial

marker E-cadherin and upregulated the mesenchymal markers N-cadherin and Vimentin in a concentration-dependent manner, thereby inducing EMT in HepG2 cells. CD2AP knockdown significantly reversed the basal EMT phenotype, increasing E-cadherin and decreasing N-cadherin and Vimentin expression. Addition of 20 ng/mL exogenous TGF-β1 significantly reversed the EMT changes induced by CD2AP knockdown and restored the cells' mesenchymal phenotype.

In Li-7 cells with low endogenous CD2AP expression, reverse rescue experiments were performed by CD2AP overexpression combined with the TβRI-specific inhibitor SB-431542 (10 μmol/L) to block TβRI kinase activity and thus verify the essential role of TβRI in the pro-tumour function of CD2AP. The wound-healing assay showed (Fig. 9E) that SB-431542 markedly inhibited the migration of CD2AP-overexpressing Li-7 cells: the 24 h relative migration distance was significantly reduced compared with the untreated group, reversing the migration enhancement induced by CD2AP overexpression. The Transwell invasion assay showed (Fig. 9F) that SB-431542 substantially decreased the number of transmembrane invasive CD2AP-overexpressing Li-7 cells ($p < 0.01$) and abrogated the invasion increase mediated by CD2AP overexpression. Western blot analysis of pathway proteins showed (Fig. 9G) that SB-431542 reduced TβRI protein levels in CD2AP-overexpressing cells and concomitantly decreased phosphorylation of downstream Smad3, thereby blocking TβRI-mediated activation of the Smad3 signalling cascade. Analysis of EMT markers showed (Fig. 9H) that SB-431542 reversed the EMT phenotype induced by CD2AP overexpression: epithelial marker E-cadherin protein expression was significantly upregulated, while mesenchymal markers N-cadherin and Vimentin were markedly downregulated. In summary, these data confirm that TβRI is indispensable for CD2AP-mediated malignant phenotypes and signalling activation in HCC cells.

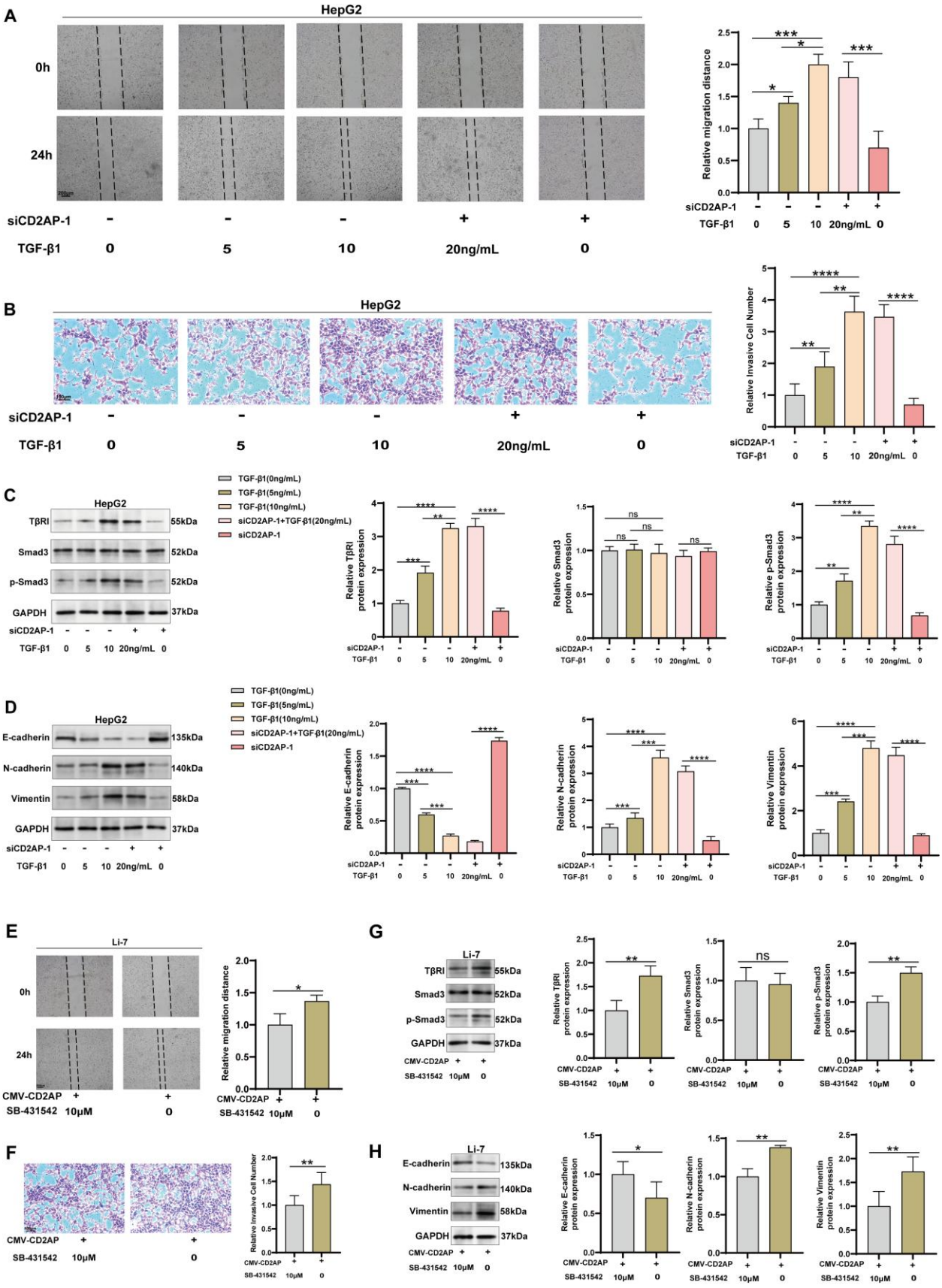

A
HepG2
0h
24h
siCD2AP-1 - - - + +
TGF-β1 0 5 10 20ng/mL 0
Relative migration distance
B
HepG2
Relative Invasive Cell Number
C
HepG2
TβRI 55kDa
Smad3 52kDa
p-Smad3 52kDa
GAPDH 37kDa
TGF-β1(0ng/mL)
TGF-β1(5ng/mL)
TGF-β1(10ng/mL)
siCD2AP-1+TGF-β1(20ng/mL)
siCD2AP-1
Relative TβRI protein expression
Relative Smad3 protein expression
Relative p-Smad3 protein expression
D
HepG2
E-cadherin 135kDa
N-cadherin 140kDa
Vimentin 58kDa
GAPDH 37kDa
Relative E-cadherin protein expression
Relative N-cadherin protein expression
Relative Vimentin protein expression
E
Li-7
CMV-CD2AP + +
SB-431542 10μM 0
Relative migration distance
G
Li-7
TβRI 55kDa
Smad3 52kDa
p-Smad3 52kDa
GAPDH 37kDa
Relative TβRI protein expression
Relative Smad3 protein expression
Relative p-Smad3 protein expression
F
Relative Invasive Cell Number
H
Li-7
E-cadherin 135kDa
N-cadherin 140kDa
Vimentin 58kDa
GAPDH 37kDa
Relative E-cadherin protein expression
Relative N-cadherin protein expression
Relative Vimentin protein expression

Fig. 9: CD2AP regulates migration, invasion, TβRI/Smad3 signaling and EMT of HCC cells in a TβRI-dependent manner. (A–B) Wound healing (A) and Transwell invasion (B) assays assessed HepG2 cell motility. Exogenous TGF-β1 promoted HepG2 migration and invasion in a concentration-dependent manner. CD2AP knockdown markedly reduced basal migration and invasion, and addition of exogenous TGF-β1 fully reversed the motility inhibition caused by CD2AP loss. (C–D) Western blotting measured pathway- and phenotype-related proteins in HepG2 cells. TGF-β1 increased TβRI, p-Smad3, and mesenchymal marker levels, while decreasing an epithelial marker in a concentration-dependent fashion. CD2AP knockdown substantially suppressed basal TβRI/Smad3 signaling and the basal EMT, and exogenous TGF-β1 restored both the signaling activity and EMT phenotype. (E–F) Wound healing (E) and Transwell invasion (F) assays evaluated motility of Li-7 cells. Treatment with the TβRI-specific inhibitor SB-431542 significantly reduced migration and invasion of CD2AP-overexpressing Li-7 cells. (G–H) Western blotting assessed pathway- and phenotype-related protein expression in Li-7 cells. SB-431542 markedly decreased TβRI and phosphorylated Smad3 levels and reversed EMT marker changes induced by CD2AP overexpression. Data are presented as mean ± SD. ns, not significant; *$p < 0.05$, **$p < 0.01$, ***$p < 0.001$, ****$p < 0.0001$.

3.10. CD2AP Drives HCC Tumor Growth via TβRI/Smad3 Activation and EMT

To validate the oncogenic function of CD2AP in vivo, subcutaneous xenograft models were generated using HepG2 cells with stable CD2AP knockdown and LI-7 cells with stable CD2AP overexpression. Tumor growth was monitored over four weeks. CD2AP knockdown in HepG2 cells markedly suppressed tumor growth compared to the control group (Fig. 10A), which was further corroborated by reduced bioluminescence signal intensity in IVIS imaging (Fig. 10B). At the molecular level, tumors derived from CD2AP-knockdown cells exhibited significantly decreased protein levels of TβRI and p-Smad3 (Fig. 10C). Consistent with the attenuation of EMT, these tumors showed upregulated epithelial marker E-cadherin and downregulated mesenchymal marker N-cadherin, which further validated that CD2AP positively regulates the

TGF-β1/Smad3 pathway activity and EMT phenotype via TβRI *in vivo*(Fig. 10D).

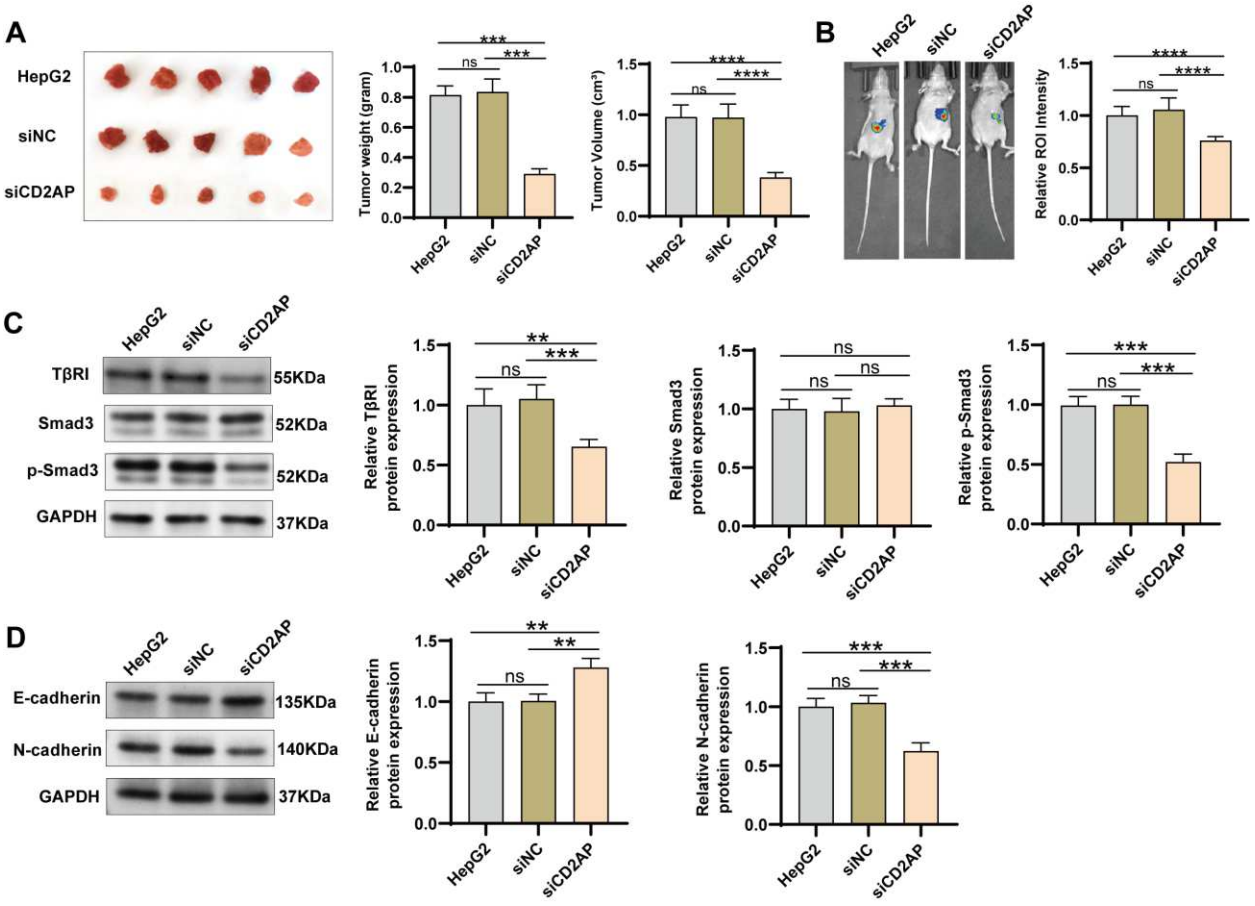


Fig. 10: CD2AP knockdown attenuates HCC tumor growth and suppresses the TβRI/Smad3-EMT axis *in vivo*. (A) Tumor growth curves demonstrate that stable knockdown of CD2AP significantly inhibits subcutaneous tumor formation in nude mice. (B) Representative in vivo bioluminescence images and quantification of total flux confirm reduced tumor burden in the CD2AP-knockdown group. (C) Western blot analysis of excised tumors shows that CD2AP depletion decreases protein levels of TβRI and phospho-Smad3 (p-Smad3). (D) Concomitantly, CD2AP knockdown reverses the EMT phenotype, elevating E-cadherin and reducing N-cadherin expression. Data are presented as mean ± SD. ns, not significant; *$p < 0.05$, **$p < 0.01$, ***$p < 0.001$, ****$p < 0.0001$.

Consistent with its proposed oncogenic role, stable overexpression of CD2AP in LI-7 cells significantly promoted subcutaneous tumor growth in nude mice compared to vector controls (Fig. 11A). This accelerated growth was further confirmed by in vivo imaging, which revealed a

pronounced increase in bioluminescence signal intensity in the CD2AP-overexpression group (Fig. 11B). At the molecular level, tumors overexpressing CD2AP exhibited a marked upregulation of TβRI and p-Smad3 protein levels (Fig. 11C). Furthermore, CD2AP overexpression potently induced a mesenchymal shift, characterized by elevated N-cadherin and suppressed E-cadherin expression (Fig. 11D). Collectively, these in vivo data establish that CD2AP drives HCC tumorigenesis by positively regulating the TβRI/Smad3 signaling pathway and EMT program via TβRI, which is consistent with our in vitro findings.

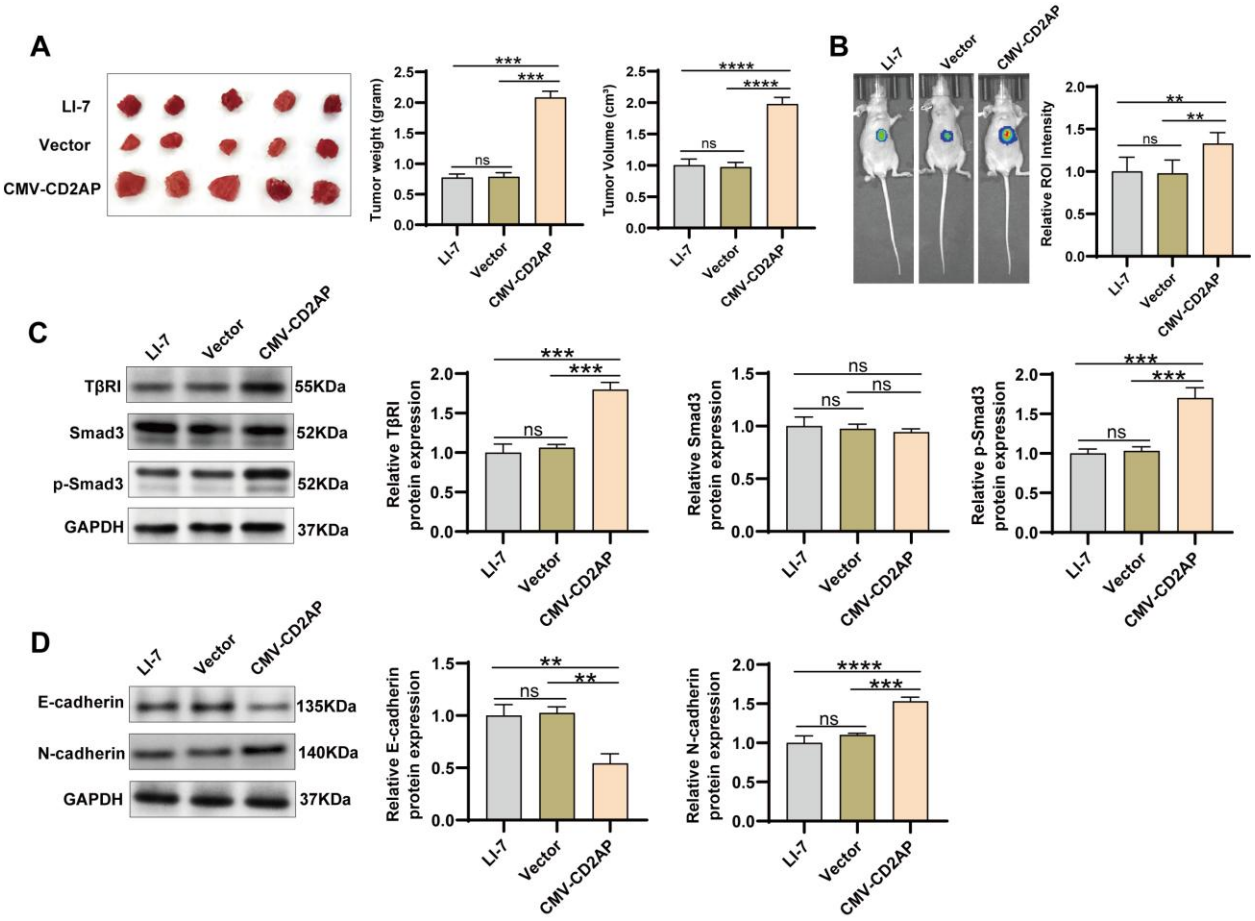


Fig. 11: CD2AP overexpression drives HCC tumor growth by activating the TβRI/Smad3-EMT axis.(A) Tumor growth kinetics demonstrate that CD2AP overexpression significantly accelerates subcutaneous tumor formation in nude mice. (B) Representative in vivo bioluminescence images and quantification of total flux confirm enhanced tumor burden in the CD2AP-overexpression group. (C) Western blot analysis of excised tumors reveals that CD2AP

upregulates protein levels of TβRI and phospho-Smad3. (D) Concomitantly, CD2AP overexpression promotes a mesenchymal phenotype, increasing N-cadherin and decreasing E-cadherin expression. Data are presented as mean ± SD. ns, not significant; *$p < 0.05$, **$p < 0.01$, ***$p < 0.001$, ****$p < 0.0001$.

4. Discussion

HCC represents a major global health burden, with a notably increasing incidence in developing countries and representing one of the leading causes of cancer-related mortality [43]. Most patients are diagnosed at advanced stages, a condition characterized by high metastatic potential and frequent drug resistance [7–9]. Although therapeutic advances have slightly improved survival rates in recent years, the inherently high malignancy, strong propensity for metastasis, and significant drug resistance of HCC continue to result in suboptimal clinical outcomes. This highly aggressive tumor is also marked by rapid recurrence and early metastatic spread [1]. These clinical challenges underscore the urgent need to elucidate the pathogenic mechanisms of HCC and highlight the critical importance of defining the core molecular drivers of its invasion and metastasis for developing novel therapeutic strategies.

The EMT is a central biological process in the development and metastatic dissemination of diverse carcinomas. Its core mechanism involves the transformation of epithelial-derived tumor cells into a mesenchymal phenotype, acquiring enhanced migratory capacity through cytoskeletal and architectural remodeling. This process is not only a pivotal pathway through which tumor cells gain motility and invasiveness but also a prerequisite for their detachment from the primary site, distant dissemination, and eventual recurrence [44,45]. Among the key pathways governing EMT, TGF-β1 plays a dominant role [46]. TGF-β1 is a multifunctional cytokine widely expressed in various cell types, including endothelial and blood cells, and exhibits a functional

duality. Under physiological conditions, it negatively regulates cell proliferation, differentiation, and immune surveillance. Conversely, within the tumor microenvironment, it promotes angiogenesis, invasion, metastasis, and host immune suppression, while also modulating apoptotic pathways [47]. The functions of TGF-β1 are primarily mediated via the canonical TGF-β/Smad3 signaling pathway: upon ligand binding to the type II receptor (TβRII) on the cell membrane, TβRII recruits and TβRI, thereby activating its serine/threonine kinase activity. This activation subsequently induces the phosphorylation of Smad3. Phosphorylated Smad3 then forms a transcriptional complex with Smad4, which translocates into the nucleus to regulate the expression of target genes [48]. Extensive studies have reported that the TGF-β/Smad3 axis promotes tumor progression in various cancers, including gastric and colorectal cancer, by modulating EMT-related molecules such as E-cadherin, N-cadherin, and Vimentin [49-53], further confirming the universal significance of this pathway in tumor metastasis. Within this cascade, Smad3 acts as the core transcriptional regulator driving malignant progression. It plays significant roles in malignancies such as colorectal, ovarian, and nasopharyngeal carcinomas. By regulating downstream targets including Notch1 and STYK1, it drives EMT, maintains cancer stemness, and contributes to chemotherapy resistance, thereby broadly enhancing the invasive and metastatic capabilities of cancer cells [54-56]. Against this background, our bioinformatic analyses revealed that CD2AP expression is significantly elevated in HCC tissues and that its high expression is closely correlated with poor patient prognosis. Further functional enrichment analysis indicated that CD2AP-related differentially expressed genes are significantly enriched in biological processes highly pertinent to tumor metastasis, notably EMT and the TGF-β signaling pathway. This suggests that CD2AP may participate in the EMT process of HCC by modulating the TGF-β1/Smad3 signaling axis, thereby influencing tumor invasion and metastasis.

TβRI occupies a pivotal position within the TGF-β signaling cascade. Owing to its high specificity and pharmacological tractability, it represents a critical target for therapeutic intervention in this pathway [57]. It fulfills key roles in diverse cancers, including pancreatic, cervical, and liver cancer. For instance, in cholangiocarcinoma cells, TβRI expression negatively correlates with the degree of cellular differentiation, peaking in undifferentiated cells [58]. In canonical signaling, TβRI is recruited to the receptor complex following TGF-β binding to TβRII; phosphorylation within its GS domain (e.g., at Ser165) activates its kinase function, initiating downstream Smad3 signaling [59]. Furthermore, TβRI engages in extensive crosstalk with multiple pathways in the tumor microenvironment. In clear cell renal cell carcinoma (ccRCC), it directly interacts with HIF-α proteins in a hypoxia-independent manner, inducing HIF-1α/2α expression and target gene activation via its kinase activity in a VHL-dependent fashion. Concurrently, HIF-α (particularly HIF-2α) provides positive feedback to amplify TGF-β signaling, establishing a bidirectional regulatory axis [60]. In ovarian cancer, TβRI can activate STAT1 (phosphorylation at S727), and the STAT1α/β isoforms, in turn, bind directly to TβRI, forming a negative feedback loop that attenuates TβRI-Smad2 signaling and significantly impacts tumor proliferation and invasion [61]. To comprehensively elucidate the regulatory effect of CD2AP on the TGF-β1/Smad3 pathway, this study employed a multifaceted experimental strategy integrating endogenous Co-IP, molecular docking, and molecular dynamics (MD) simulations. Endogenous Co-IP first confirmed a direct physical interaction between CD2AP and TβRI in HCC cells, which was further supported by molecular docking and MD simulations showing that the two proteins can form a stable complex with high binding affinity.

The dysregulated expression of the scaffold protein CD2AP is closely associated with the

development, invasion, metastasis, and prognosis of various epithelial-derived tumors. Its function exhibits remarkable cancer-type specificity: it acts as an oncoprotein in HCC and lung adenocarcinoma (LUAD) [23,24], while serving a tumor-suppressive role in ccRCC and gastric cancer [19,21,22]. This dichotomy underscores the complexity of oncogenic signaling networks, wherein the same molecule can be "functionally reprogrammed" within distinct tissue microenvironments. It further implies that therapeutic strategies targeting CD2AP must carefully consider this contextual dependency. Our study systematically clarifies the oncogenic function of CD2AP in HCC. We demonstrate experimentally that CD2AP is a key positive regulator of the TGF-β1/Smad3 signaling pathway. Its action is independent of TGF-β1 ligand regulation, but relies on its scaffold function to directly bind TβRI. Notably, CD2AP expression levels are positively correlated with TβRI protein abundance, and genetic manipulation of CD2AP synchronously modulates TβRI protein level, downstream Smad3 phosphorylation, and EMT phenotype. These findings confirm that CD2AP positively regulates the activity of the downstream TGF-β1/Smad3 signaling pathway and EMT phenotype via TβRI in HCC.

Notably, this study has several limitations. First, this study confirmed that CD2AP positively regulates TGF-β1/Smad3 signaling via TβRI, and found a positive correlation between CD2AP expression and TβRI protein abundance. However, the detailed molecular mechanism by which CD2AP modulates TβRI protein level (including but not limited to regulating protein degradation, translation, or membrane trafficking) has not been fully elucidated, which will be the focus of our follow-up research. Second, the key amino acid residues mediating the CD2AP-TβRI interaction and their specific functional roles remain to be further validated by site-directed mutagenesis.

5. Conclusion

In conclusion, this study systematically delineates the novel oncogenic function of CD2AP in HCC, and confirms that CD2AP positively regulates the activity of the downstream TGF-β1/Smad3 signaling pathway and EMT phenotype via direct interaction with TβRI, thereby promoting the malignant progression of HCC. These findings not only advance our understanding of the regulatory network of the TGF-β pathway in HCC, but also provide a solid theoretical and experimental basis for targeting the CD2AP-TβRI axis for prognostic stratification and therapeutic intervention in HCC.

Abbreviations

CD2AP: CD2-associated protein

HCC: Hepatocellular carcinoma

EMT: Epithelial-mesenchymal transition

TGF-β1: Transforming growth factor-β1

Co-IP: Co-Immunoprecipitation

TβRI: TGF-β receptor type I

TCGA: The Cancer Genome Atlas

GTEx: Genotype-Tissue Expression

TPM: Transcripts per million

DEGs: Differentially Expressed Genes

GO: Gene Ontology

KEGG: Kyoto Encyclopedia of Genes and Genomes

OS: Overall survival

DSS: Disease-specific survival

PFI: Progression-free interval

FBS: Fetal bovine serum

PBS: Phosphate-buffered saline

siRNA: Small interfering RNA

siNC: Non-targeting control siRNA

shRNA: Short hairpin RNA

shControl: Non-targeting control shRNA

CCK-8: Cell Counting Kit-8

PVDF: Polyvinylidene difluoride

TBST: Tris-buffered saline containing 0.1% Tween-20

BSA: Bovine serum albumin

HRP: Horseradish peroxidase

ECL: Enhanced chemiluminescence

IF: Immunofluorescence

ZO-1: Zonula Occludens-1

DAPI: 4',6-diamidino-2-phenylindole

MD: Molecular dynamics

PME: Particle Mesh Ewald

IVIS: In Vivo Imaging System

ROI: Region of interest

ROC: Receiver operating characteristic

AUC: Area under the curve

CI: Confidence interval

HR: Hazard ratio

PLIP: Protein–Ligand Interaction Profiler

FEL: Free-energy landscape

ccRCC: Clear cell renal cell carcinoma

LUAD: Lung adenocarcinoma

RMSD: Root-mean-square deviation

RMSF: Root-mean-square fluctuation

Rg: Radius of gyration

SASA: Solvent-accessible surface area

Acknowledgements

Not applicable.

Funding

This work was supported by the Affiliated Hospital of Traditional Chinese Medicine of Xinjiang Medical University.

Authors Contributions

D Wang: Cell experiments and data analysis; X Meng: Clinical cohort analysis and data processing; F Fan: Molecular biology experiments and data analysis; D Tuerhong: In vivo animal experiments and data analysis; Y Li and J Liu：Molecular docking and dynamics simulations with data analysis; S Zhao: Assisted in study design, data interpretation and

manuscript drafting; H Zhang: Study conception and design, funding acquisition, research supervision and manuscript revision. All authors read and approved the final manuscript.

Ethics declarations

Ethics approval and consent to participate

Clinical trial number: not applicable. All animal experiments were conducted in accordance with the National Institutes of Health Guide for the Care and Use of Laboratory Animals. Experimental protocols were reviewed and approved by the Laboratory Animal Ethics Committee of Xinjiang Medical University (Approval No. XJMU-IACUC-20260123-04; Date: 23 January 2026). The committee operates in compliance with the International Council for Laboratory Animal Science (ICLAS) guidelines (approved by the ICLAS Governing Board on 6 June 2013). All procedures were performed in strict accordance with institutional care and use guidelines to ensure compliance with international ethical standards.

Consent for publication

Not applicable.

Competing interests

The authors declare no competing interests.

Data availability

The original data generated by this study can be reasonably requested from the

corresponding author.

Code availability

No custom code was generated or used in the present study.

References

1. European Association for the Study of the Liver. EASL Clinical Practice Guidelines: Management of hepatocellular carcinoma. J Hepatol. 2018;69(1):182-236. https://doi.org/10.1016/j.jhep.2018.03.019.
2. Chan YT, Zhang C, Wu J, Lu P, Xu L, Yuan H, et al. Biomarkers for diagnosis and therapeutic options in hepatocellular carcinoma. Mol Cancer. 2024;23(1):189. https://doi.org/10.1186/s12943-024-02101-z.
3. Zhang L, Xu J, Zhou S, Yao F, Zhang R, You W, et al. Endothelial DGKG promotes tumor angiogenesis and immune evasion in hepatocellular carcinoma. J Hepatol. 2024;80(1):82-98. https://doi.org/10.1016/j.jhep.2023.10.006.
4. Gordan JD, Kennedy EB, Abou-Alfa GK, Beal E, Finn RS, Gade TP, et al. Systemic Therapy for Advanced Hepatocellular Carcinoma: ASCO Guideline Update. J Clin Oncol. 2024;42(15):1830-1850. https://doi.org/10.1200/JCO.23.02745.
5. Parikh ND, Patel R, Hu J, Stirnadel-Farrant HA, Kebede N, Wang C, et al. Real-world treatment patterns and outcomes in patients with early-stage HCC in the US treated with resection or ablation. Hepat Oncol. 2025;12(1):2530377. https://doi.org/10.1080/20450923.2025.2530377.
6. Saowapa S, Polpichai N, Danpanichkul P, Bernal RB, Siladech P, Tijani L, et al. Comparative

Efficacy and Safety of First-Line Treatment With Atezolizumab/Bevacizumab vs. Tyrosine-kinase Inhibitors in Patients With Unresectable Hepatocellular Carcinoma: A Systematic Review and Meta-analysis. J Clin Exp Hepatol. 2025;15(6):102633. https://doi.org/10.1016/j.jceh.2025.102633.

7. Zhai Y, Wang L, Zhao H, Wu F, Xin L, Ye F, et al. Phase II study with sorafenib plus radiotherapy for advanced HCC with portal and/or hepatic vein tumor thrombosis. JHEP Rep. 2024;7(3):101287. https://doi.org/10.1016/j.jhepr.2024.101287.
8. Liu M, Liu Y, Zheng J, An X, Wen J, Zhu F, et al. Targeting STARD4/EGFR axis inhibits growth and overcomes lenvatinib resistance in hepatocellular carcinoma. Genes Dis. 2025;12(6):101556. https://doi.org/10.1016/j.gendis.2025.101556.
9. Zhu L, Zu M, Wu F, Ma X, Zhang S, Zhang T, et al. Cancer-associated fibroblasts regulating nanomedicine to overcome sorafenib resistance in hepatocellular carcinoma with portal vein tumor thrombus. Biomaterials. 2026;325:123599. https://doi.org/10.1016/j.biomaterials.2025.123599.
10. Misri G, Murakonda AB, Naslavsky N, Caplan S. CIN85 and CD2AP Are Novel Constituents of Dynamic Tubular Recycling Endosomes That Regulate Recycling Upon Recruitment by MICAL-L1. Traffic. 2025;26(7-9):e70015. https://doi.org/10.1111/tra.70015.
11. Schaefer A, van Duijn TJ, Majolee J, Burridge K, Hordijk PL. Endothelial CD2AP Binds the Receptor ICAM-1 To Control Mechanosignaling, Leukocyte Adhesion, and the Route of Leukocyte Diapedesis In Vitro. J Immunol. 2017;198(12):4823-4836. https://doi.org/10.4049/jimmunol.1601987.
12. Wang Y, Brieher WM. CD2AP links actin to PI3 kinase activity to extend epithelial cell

height and constrain cell area. J Cell Biol. 2020;219(1):e201812087. https://doi.org/10.1083/jcb.201812087.

13. Ao Y, Yang F, Li J, Gong X, Liu H, Wu Y, et al. Cryptosporidium dense granule effector MUC5 interacts with host actin cytoskeleton through CD2AP. Microbiol Res. 2025;300:128284. https://doi.org/10.1016/j.micres.2025.128284.
14. Tossidou I, Teng B, Worthmann K, Müller-Deile J, Jobst-Schwan T, Kardinal C, et al. Tyrosine Phosphorylation of CD2AP Affects Stability of the Slit Diaphragm Complex. J Am Soc Nephrol. 2019;30(7):1220-1237. https://doi.org/10.1681/ASN.2018080860.
15. van Duijn TJ, Anthony EC, Hensbergen PJ, Deelder AM, Hordijk PL. Rac1 recruits the adapter protein CMS/CD2AP to cell-cell contacts. J Biol Chem. 2010;285(26):20137-20146. https://doi.org/10.1074/jbc.M109.099481.
16. Vandal M, Janmaleki M, Rea I, Gunn C, Hirai S, Biernaskie J, et al. CD2AP at the junction of nephropathy and Alzheimer's disease. Mol Neurodegener. 2025;20(1):63. https://doi.org/10.1186/s13024-025-00852-x.
17. Tolvanen TA, Dash SN, Polianskyte-Prause Z, Dumont V, Lehtonen S. Lack of CD2AP disrupts Glut4 trafficking and attenuates glucose uptake in podocytes. J Cell Sci. 2015 Dec 15;128(24):4588-600. https://doi.org/10.1242/jcs.175075.
18. Camacho J, Rábano A, Marazuela P, Bonaterra-Pastra A, Serna G, Molinè T, et al. Association of CD2AP neuronal deposits with Braak neurofibrillary stage in Alzheimer's disease. Brain Pathol. 2022;32(1):e13016. https://doi.org/10.1111/bpa.13016.
19. Chen C, Xu J, Zhang JX, Chen LY, Wei YA, Zhang WM, et al. CD2AP is a potential prognostic biomarker of renal clear cell carcinoma. Cancer Med. 2024;13(4):e7055. https://doi.org/10.1002/cam4.7055.

20. Kurilla A, László L, Takács T, Tilajka Á, Lukács L, Novák J, et al. Studying the Association of TKS4 and CD2AP Scaffold Proteins and Their Implications in the Partial Epithelial-Mesenchymal Transition (EMT) Process. Int J Mol Sci. 2023;24(20):15136. https://doi.org/10.3390/ijms242015136.

21. Li H, Chen H, Zhao T, Zhang W, Deng J, Xie W, et al. CD2AP shapes a stromal reduced tumor microenvironment and contributes to immunotherapy in gastric cancer. BMC Cancer. 2025;25(1):910. https://doi.org/10.1186/s12885-025-14248-z.

22. Xie W, Chen C, Han Z, Huang J, Liu X, Chen H, et al. CD2AP inhibits metastasis in gastric cancer by promoting cellular adhesion and cytoskeleton assembly. Mol Carcinog. 2020;59(4):339-352. https://doi.org/10.1002/mc.23158.

23. Lin Z, Lv J, Dai C, Zhai Y, Jiang J, Gao Y, et al. Identification of the disulfidptosis-related key gene CD2AP as a potential biomarker and new therapeutic target for LUAD patients by comprehensive multi-omics analysis. Discov Oncol. 2025;16(1):515. https://doi.org/10.1007/s12672-025-02308-6.

24. Shang N, Wang J, Liu Z, Wang Y, Zhang D, Liu H, et al. Integrated Analysis of Disulfidptosis-Related Genes Identifies CD2AP as a Potential Therapeutic Target for Hepatocellular Carcinoma. Int J Mol Sci. 2025;26(9):4454. https://doi.org/10.3390/ijms26094454.

25. Ashrafizadeh M, Dai J, Torabian P, Nabavi N, Aref AR, Aljabali AAA, et al. Circular RNAs in EMT-driven metastasis regulation: modulation of cancer cell plasticity, tumorigenesis and therapy resistance. Cell Mol Life Sci. 2024;81(1):214. https://doi.org/10.1007/s00018-024-05236-w.

26. Xue W, Yang L, Chen C, Ashrafizadeh M, Tian Y, Sun R. Wnt/β-catenin-driven EMT

regulation in human cancers. Cell Mol Life Sci. 2024;81(1):79. https://doi.org/10.1007/s00018-023-05099-7.=-5111.

27. Hu Z, Sui Q, Jin X, Shan G, Huang Y, Yi Y, et al. IL6-STAT3-C/EBPβ-IL6 positive feedback loop in tumor-associated macrophages promotes the EMT and metastasis of lung adenocarcinoma. J Exp Clin Cancer Res. 2024;43(1):63. https://doi.org/10.1186/s13046-024-02989-x.
28. Ebrahimi N, Manavi MS, Faghihkhorasani F, Fakhr SS, Baei FJ, Khorasani FF, et al. Harnessing function of EMT in cancer drug resistance: a metastasis regulator determines chemotherapy response. Cancer Metastasis Rev. 2024;43(1):457-479. https://doi.org/10.1007/s10555-023-10162-7.
29. Saitoh M. Transcriptional regulation of EMT transcription factors in cancer. Semin Cancer Biol. 2023;97:21-29. https://doi.org/10.1016/j.semcancer.2023.10.001.
30. Lengrand J, Pastushenko I, Vanuytven S, Song Y, Venet D, Sarate RM, et al. Pharmacological targeting of netrin-1 inhibits EMT in cancer. Nature. 2023;620(7973):402-408. https://doi.org/10.1038/s41586-023-06372-2.
31. Wang X, Eichhorn PJA, Thiery JP. TGF-β, EMT, and resistance to anti-cancer treatment. Semin Cancer Biol. 2023;97:1-11. https://doi.org/10.1016/j.semcancer.2023.10.004.
32. Zhang YE, Stuelten CH. Alternative splicing in EMT and TGF-β signaling during cancer progression. Semin Cancer Biol. 2024;101:1-11. https://doi.org/10.1016/j.semcancer.2024.04.001.
33. Fawzy MA, Beshay ON, Bekhit AA, Abdel-Hafez SMN, Batiha GE, Bin Jardan YA, et al. Nephroprotective effect of AT-MSCs against cisplatin-induced EMT is improved by

azilsartan via attenuating oxidative stress and TGF-β/Smad signaling. Biomed Pharmacother. 2023;158:114097. https://doi.org/10.1016/j.biopha.2022.114097.

34. Xavier S, Niranjan T, Krick S, Zhang T, Ju W, Shaw AS, et al. TbetaRI independently activates Smad- and CD2AP-dependent pathways in podocytes. J Am Soc Nephrol. 2009;20(10):2127-2137. https://doi.org/10.1681/ASN.2008070806.
35. Colaprico A, Silva TC, Olsen C, Garofano L, Cava C, Garolini D, et al. TCGAbiolinks: an R/Bioconductor package for integrative analysis of TCGA data. Nucleic Acids Res. 2016;44(8):e71. https://doi.org/10.1093/nar/gkv1507.
36. GTEx Consortium. The GTEx Consortium atlas of genetic regulatory effects across human tissues. Science. 2020;369(6509):1318-1330. https://doi.org/10.1126/science.aaz1776.
37. Goldman MJ, Craft B, Hastie M, Repečka K, McDade F, Kamath A, et al. Visualizing and interpreting cancer genomics data via the Xena platform. Nat Biotechnol. 2020;38(6):675-678. https://doi.org/10.1038/s41587-020-0546-8.
38. Love MI, Huber W, Anders S. Moderated estimation of fold change and dispersion for RNA-seq data with DESeq2. Genome Biol. 2014;15(12):550. https://doi.org/10.1186/s13059-014-0550-8.
39. Walter W, Sánchez-Cabo F, Ricote M. GOplot: an R package for visually combining expression data with functional analysis. Bioinformatics. 2015;31(17):2912-2914. https://doi.org/10.1093/bioinformatics/btv300.
40. Ahmad S, Jose da Costa Gonzales L, Bowler-Barnett EH, Rice DL, Kim M, Wijerathne S, et al. The UniProt website API: facilitating programmatic access to protein knowledge. Nucleic Acids Res. 2025;53(W1):W547-W553. https://doi.org/10.1093/nar/gkaf394.
41. Yan Y, Tao H, He J, Huang SY. The HDOCK server for integrated protein-protein

docking. Nat Protoc. 2020;15(5):1829-1852. https://doi.org/10.1038/s41596-020-0312-x.

42. Valdés-Tresanco MS, Valdés-Tresanco ME, Valiente PA, Moreno E. gmx_MMPBSA: A New Tool to Perform End-State Free Energy Calculations with GROMACS. J Chem Theory Comput. 2021;17(10):6281-6291. https://doi.org/10.1021/acs.jctc.1c00645.

43. Zhu H, Zhao Y, Wang Y, Wei G, Liu J. Understanding the relationship between cuproptosis and the development of hepatocellular carcinoma: implications for targeted therapies. Front Immunol. 2025;16:1557223. https://doi.org/10.3389/fimmu.2025.1557223.

44. Chaffer CL, San Juan BP, Lim E, Weinberg RA. EMT, cell plasticity and metastasis. Cancer Metastasis Rev. 2016;35(4):645-654. https://doi.org/10.1007/s10555-016-9648-7.

45. Lambert AW, Weinberg RA. Linking EMT programmes to normal and neoplastic epithelial stem cells. Nat Rev Cancer. 2021;21(5):325-338. https://doi.org/10.1038/s41568-021-00332-6.

46. Kim BN, Ahn DH, Kang N, Yeo CD, Kim YK, Lee KY, et al. TGF-β induced EMT and stemness characteristics are associated with epigenetic regulation in lung cancer. Sci Rep. 2020;10(1):10597. https://doi.org/10.1038/s41598-020-67325-7.

47. de Streel G, Lucas S. Targeting immunosuppression by TGF-β1 for cancer immunotherapy. Biochem Pharmacol. 2021;192:114697. https://doi.org/10.1016/j.bcp.2021.114697.

48. Ding J, Yang YY, Li PT, Ma Y, Zhang L, Zhou Y, et al. TGF-β1/SMAD3-driven GLI2 isoform expression contributes to aggressive phenotypes of hepatocellular carcinoma. Cancer Lett. 2024;588:216768. https://doi.org/10.1016/j.canlet.2024.216768.

49. Yang Z, Zhang H, Yin M, Cheng Z, Jiang P, Feng M, et al. TGF-β1/Smad3 upregulates UCA1 to promote liver fibrosis through DKK1 and miR18a. J Mol Med (Berl).

2022;100(10):1465-1478. https://doi.org/10.1007/s00109-022-02248-6.

50. Hu W, Zheng X, Liu J, Zhang M, Liang Y, Song M. MicroRNA MiR-130a-3p promotes gastric cancer by targeting Glucosaminyl N-acetyl transferase 4 (GCNT4) to regulate the TGF-β1/SMAD3 pathway. Bioengineered. 2021;12(2):11634-11647. https://doi.org/10.1080/21655979.2021.1995099.

51. Zhu C, Teng L, Lai Y, Yao X, Fang Y, Wang Z, et al. Adipose-derived stem cells promote glycolysis and peritoneal metastasis via TGF-β1/SMAD3/ANGPTL4 axis in colorectal cancer. Cell Mol Life Sci. 2024;81(1):189. https://doi.org/10.1007/s00018-024-05215-1.

52. Zhang G, Yu T, Chai X, Zhang S, Liu J, Zhou Y, et al. Gradient Rotating Magnetic Fields Impairing F-Actin-Related Gene CCDC150 to Inhibit Triple-Negative Breast Cancer Metastasis by Inactivating TGF-β1/SMAD3 Signaling Pathway. Research (Wash D C). 2024;7:0320. https://doi.org/10.34133/research.0320.

53. Deng L, Bao W, Zhang B, Zhang S, Chen Z, Zhu X, et al. AZGP1 activation by lenvatinib suppresses intrahepatic cholangiocarcinoma epithelial-mesenchymal transition through the TGF-β1/Smad3 pathway. Cell Death Dis. 2023;14(9):590. https://doi.org/10.1038/s41419-023-06092-5.

54. Shi Y, Zhang J, Liu M, Huang Y, Yin L. SMAD3 inducing the transcription of STYK1 to promote the EMT process and improve the tolerance of ovarian carcinoma cells to paclitaxel. J Cell Biochem. 2019;120(6):10796-10811. https://doi.org/10.1002/jcb.28371.

55. Clark AG, Bertrand FE, Sigounas G. A potential requirement for Smad3 phosphorylation in Notch-mediated EMT in colon cancer. Adv Biol Regul. 2023;88:100957. https://doi.org/10.1016/j.jbior.2023.100957.

56. Zhao C, Zhao F, Feng H, Xu S, Qin G. MicroRNA-92b inhibits epithelial-mesenchymal

transition-induced migration and invasion by targeting Smad3 in nasopharyngeal cancer. Oncotarget. 2017;8(53):91603-91613. https://doi.org/10.18632/oncotarget.21342.

57. Shen N, Shao Z, Xin H, Che F, Cui Y. Exploring TβRI inhibitors from Arenaria kansuensis based on 3D-QSAR, molecular docking and molecular dynamics simulation methods and its anti-pulmonary fibrosis molecular mechanism validation. J Ethnopharmacol. 2025;337(Pt 1):118788. https://doi.org/10.1016/j.jep.2024.118788.

58. Zhang Q, Zhou J, Zhai D, Jiang Q, Yang M, Zhou M. Gut microbiota regulates the ALK5/NOX1 axis by altering glutamine metabolism to inhibit ferroptosis of intrahepatic cholangiocarcinoma cells. Biochim Biophys Acta Mol Basis Dis. 2024;1870(5):167152. https://doi.org/10.1016/j.bbadis.2024.167152.

59. Huang T, David L, Mendoza V, Yang Y, Villarreal M, De K, et al. TGF-β signalling is mediated by two autonomously functioning TβRI:TβRII pairs. EMBO J. 2011;30(7):1263-1276. https://doi.org/10.1038/emboj.2011.54.

60. Mallikarjuna P, Raviprakash TS, Aripaka K, Ljungberg B, Landström M. Interactions between TGF-β type I receptor and hypoxia-inducible factor-α mediates a synergistic crosstalk leading to poor prognosis for patients with clear cell renal cell carcinoma. Cell Cycle. 2019;18(17):2141-2156. https://doi.org/10.1080/15384101.2019.1642069.

61. Tian X, Guan W, Zhang L, Sun W, Zhou D, Lin Q, et al. Physical interaction of STAT1 isoforms with TGF-β receptors leads to functional crosstalk between two signaling pathways in epithelial ovarian cancer. J Exp Clin Cancer Res. 2018;37(1):103. https://doi.org/10.1186/s13046-018-0773-8.

Supplementary Files

This is a list of supplementary files associated with this preprint. Click to download.

- OriginalWesternBlots.pdf